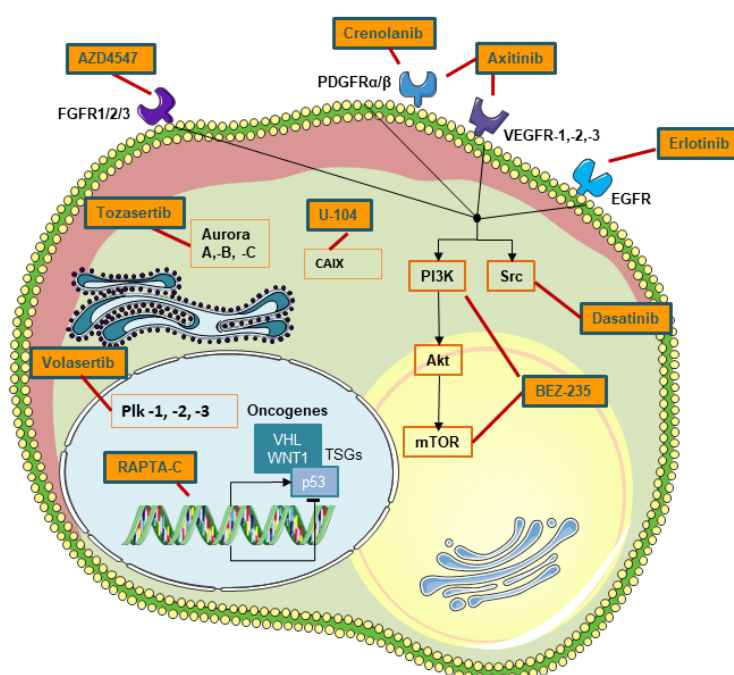


Supplementary Figures

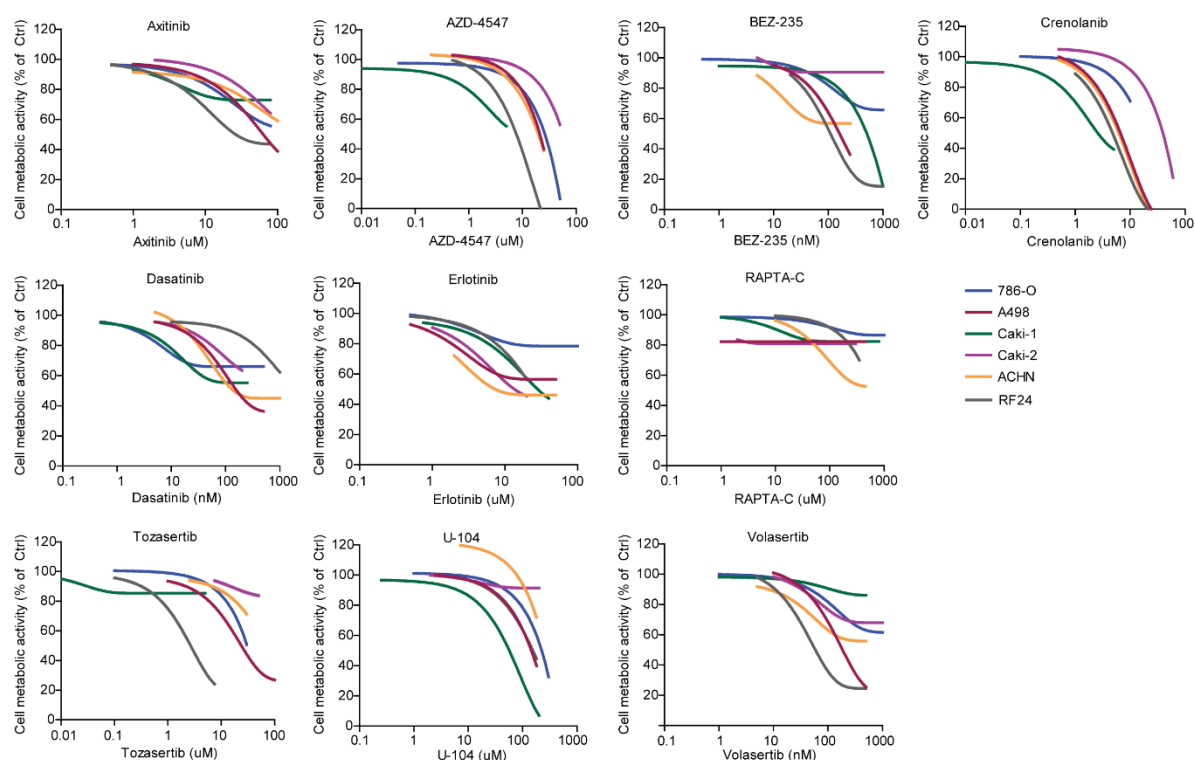
# Integrating phenotypic search and phosphoproteomic profiling of active kinases for optimization of drug mixtures for RCC treatment

Judy R. van Beijnum, Andrea Weiss, Robert H. Berndsen, Tse J. Wong, Louise C. Reckman, Sander R. Piersma, Marloes Zoetemelk, Richard de Haas, Olivier Dormond, Axel Bex, Alexander A. Henneman, Connie R. Jimenez, Arjan W. Griffioen, Patrycja Nowak-Sliwinska

Supplement 1: s-FSC of RCC lines

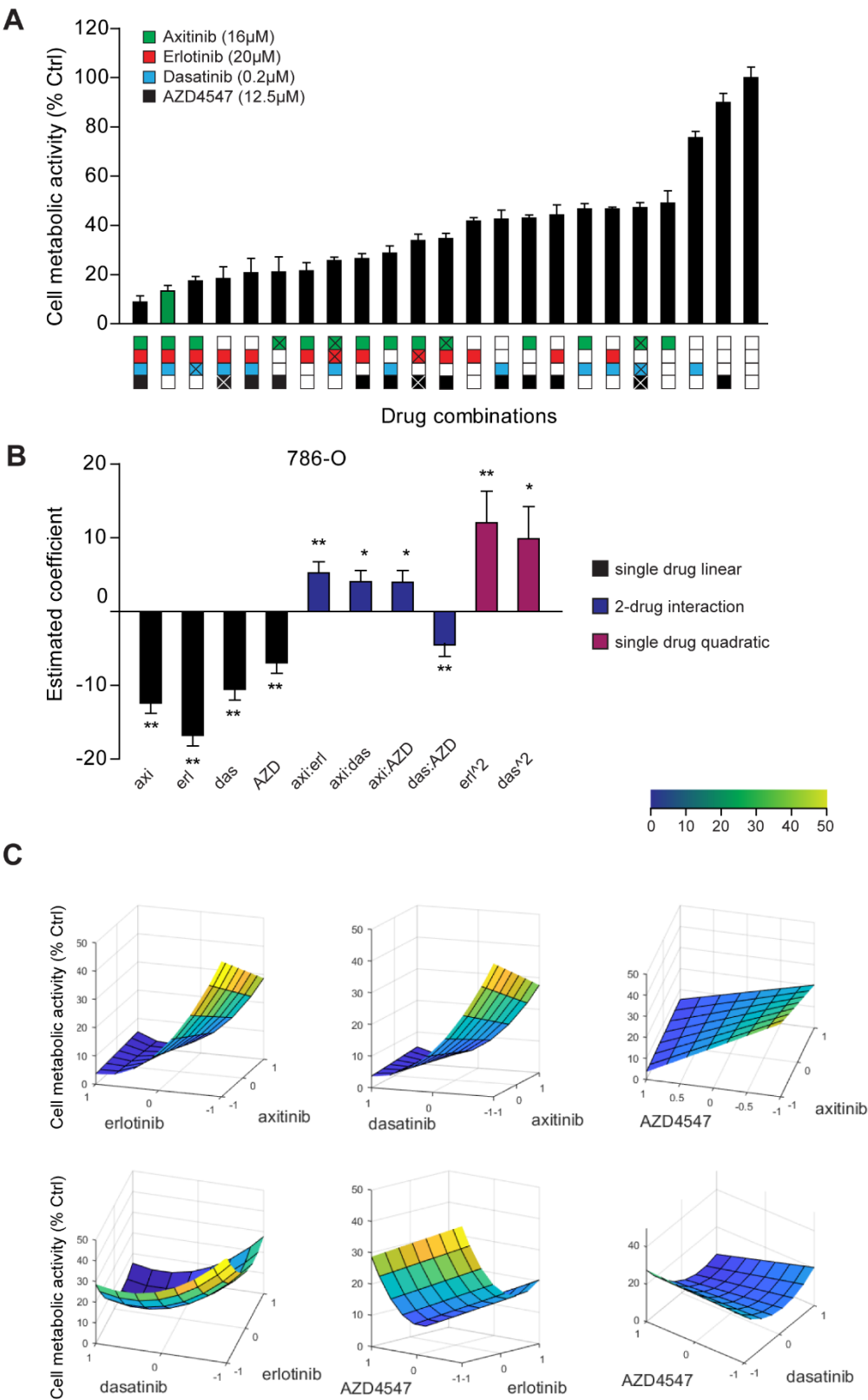


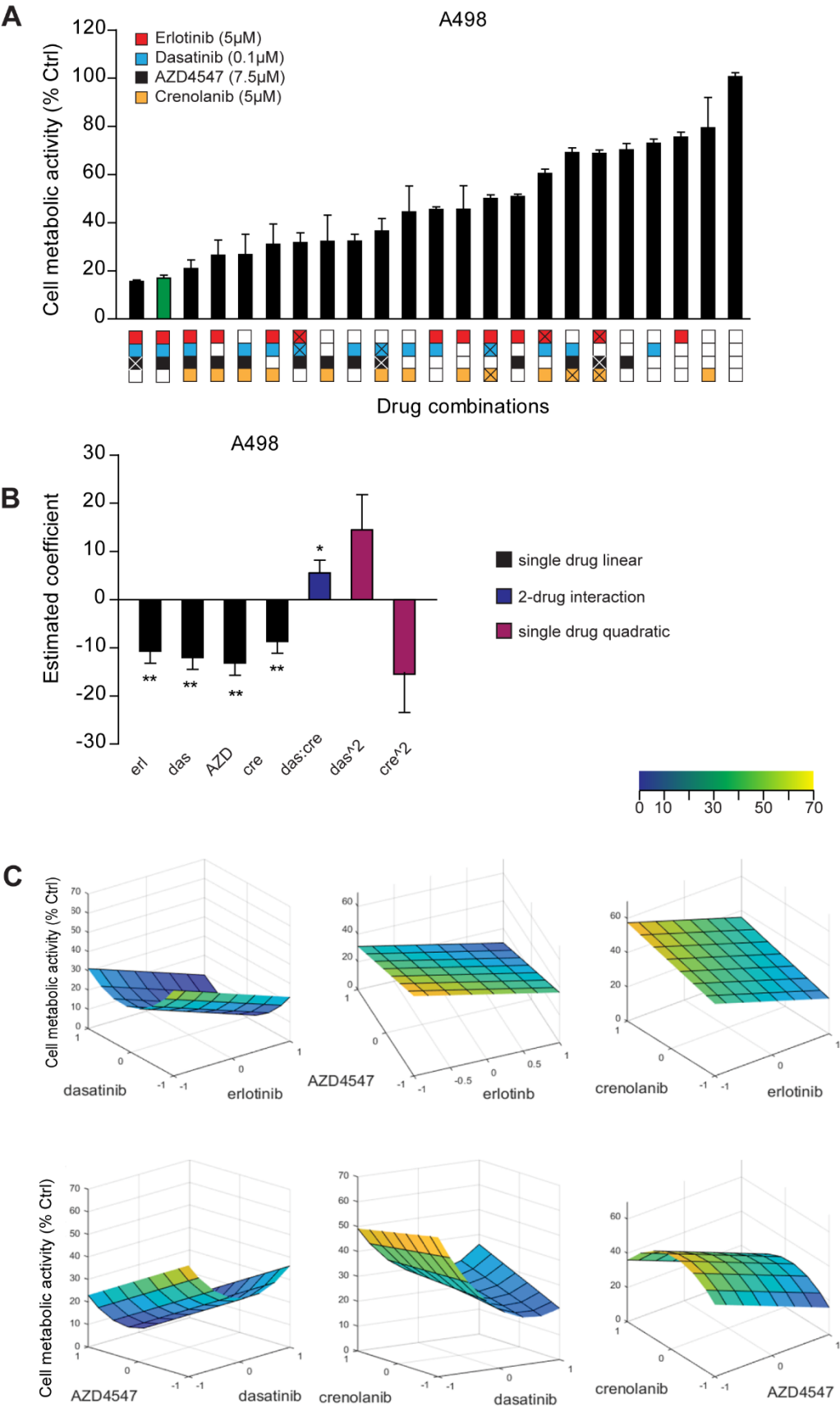
**Figure S1.1.1.** Drug selection. Schematic drawing of ten initial drugs covering a broad targeting spectrum in a cell: axitinib (VEGFR's, PDGFR and c-KIT); erlotinib (EGFR inhibitor); RAPTA-C (chromatin inactivator); BEZ-235 (inhibitor of both of the main protein complexes of mTOR (mechanistic target of rapamycin), mTORC1 and mTORC2); volasertib (inhibitor of PLK- polo-like kinase, which is found in the nuclei of dividing cells, and controls multiple stages of cell cycle and division); dasatinib (inhibitor of BCR/ABL and Src, binding both active and inactive forms of ABL kinase); tozasertib (VX-680, inhibitor of Aurora A, B, C, which play a role in mitosis and meiosis during proliferation (between G2 to M phase); U-104 (inhibitor of carbonic anhydrase IX/X inhibitor II. CAIX expression is regulated by VHL protein, and VHL mutation loss is associated with clear cell RCC, so CAIX expression is related to clear cell RCC); AZD4547 (TKI targeting FGFR 1-3 and also showing a weak activity against FGFR4), and crenolanib (designed to inhibit PDGFRs but shown to act via cell cycle modulation as well).



**Figure S1.1.2.** Monotherapy dose response curves. Dose response curves based on cell metabolic activity were generated for 5 RCC lines (786-O, A498, Caki-1, Caki-2 and ACHN) and the endothelial cell line EC-RF24, for all ten drugs used in the s-FSC screen. For presentation purposes, non-linear fitting was performed on the data (at least triplicate measurements). Experiments were performed in triplicate and repeated 2–4 times per condition.

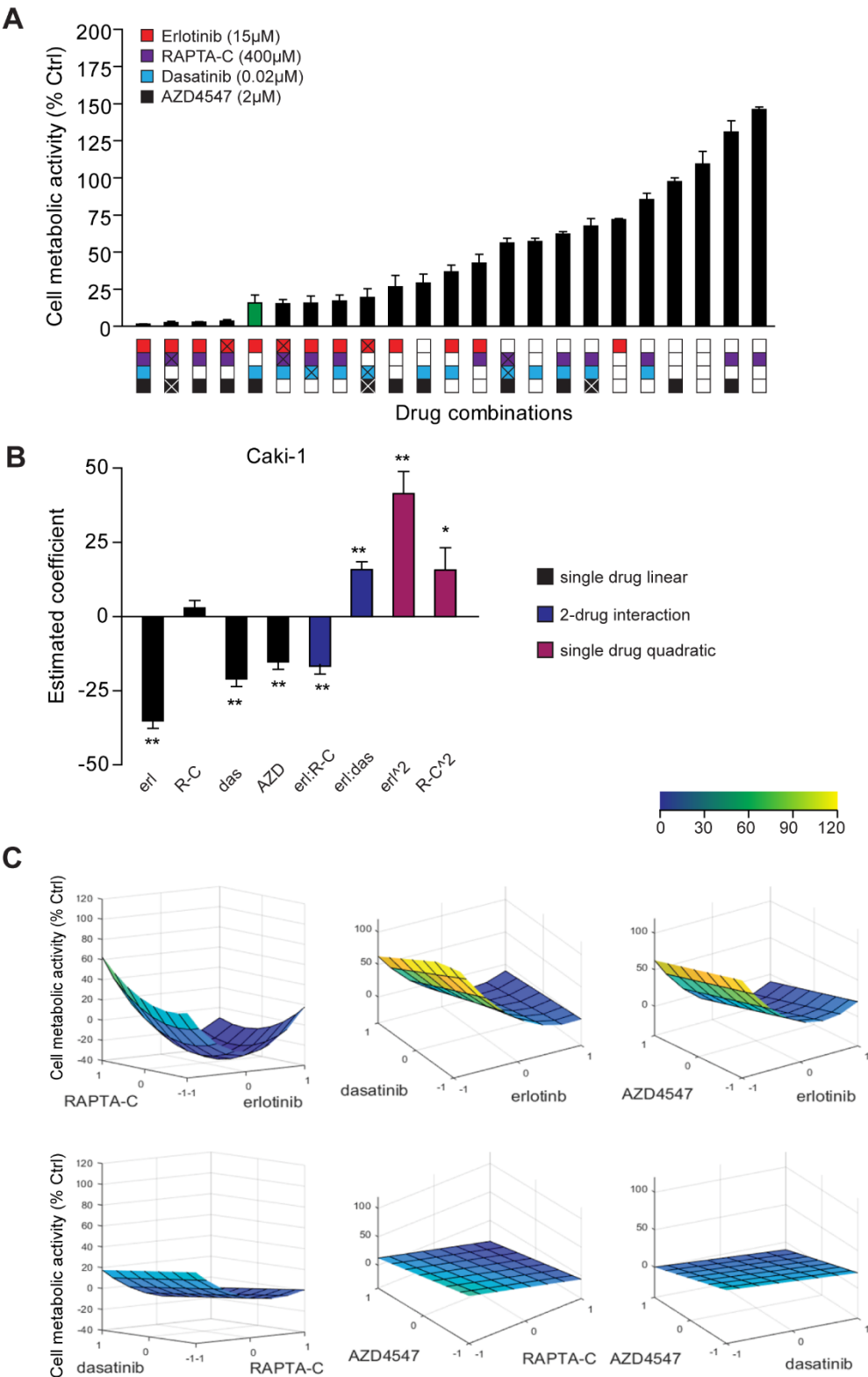
786-O

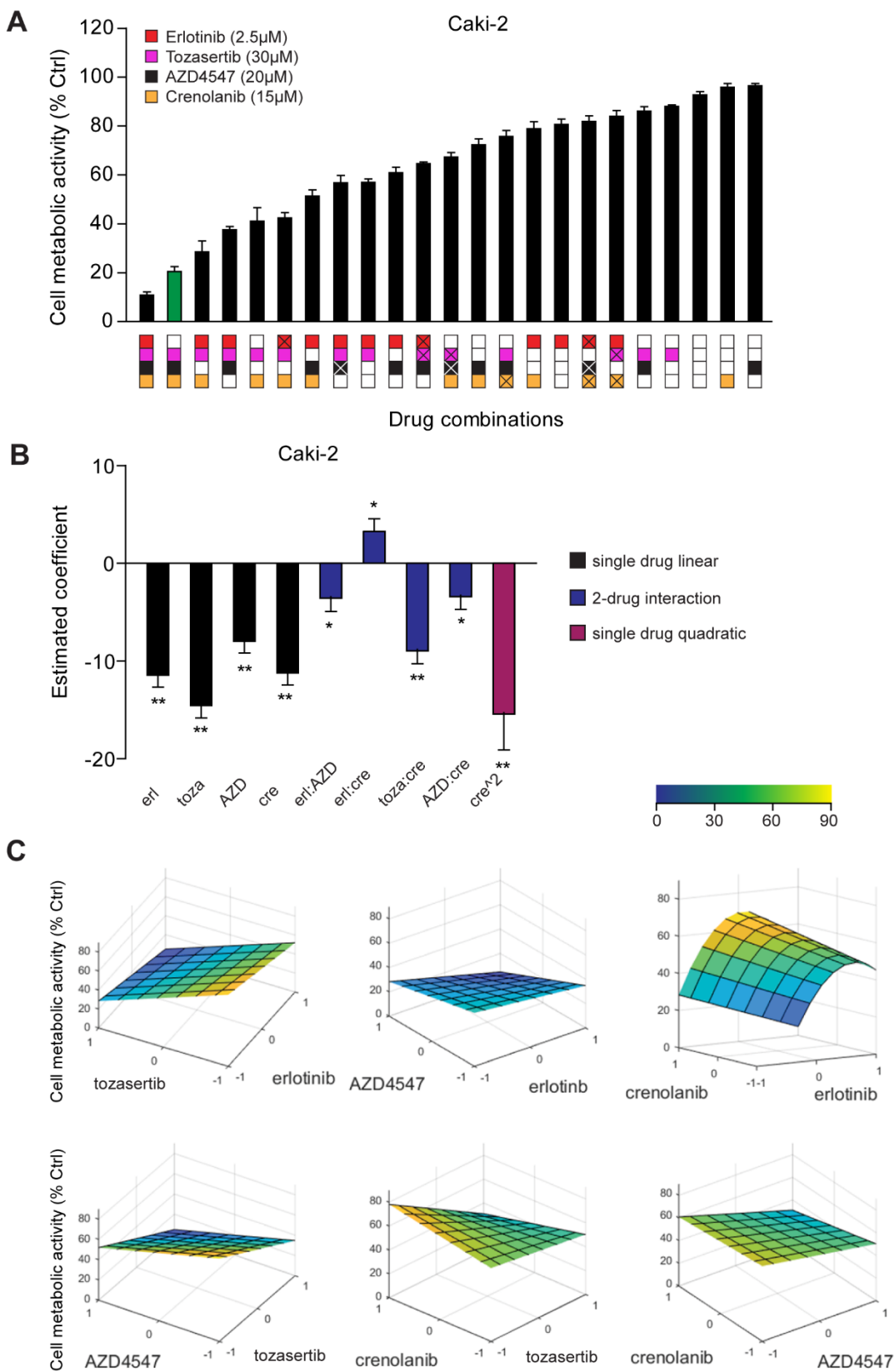


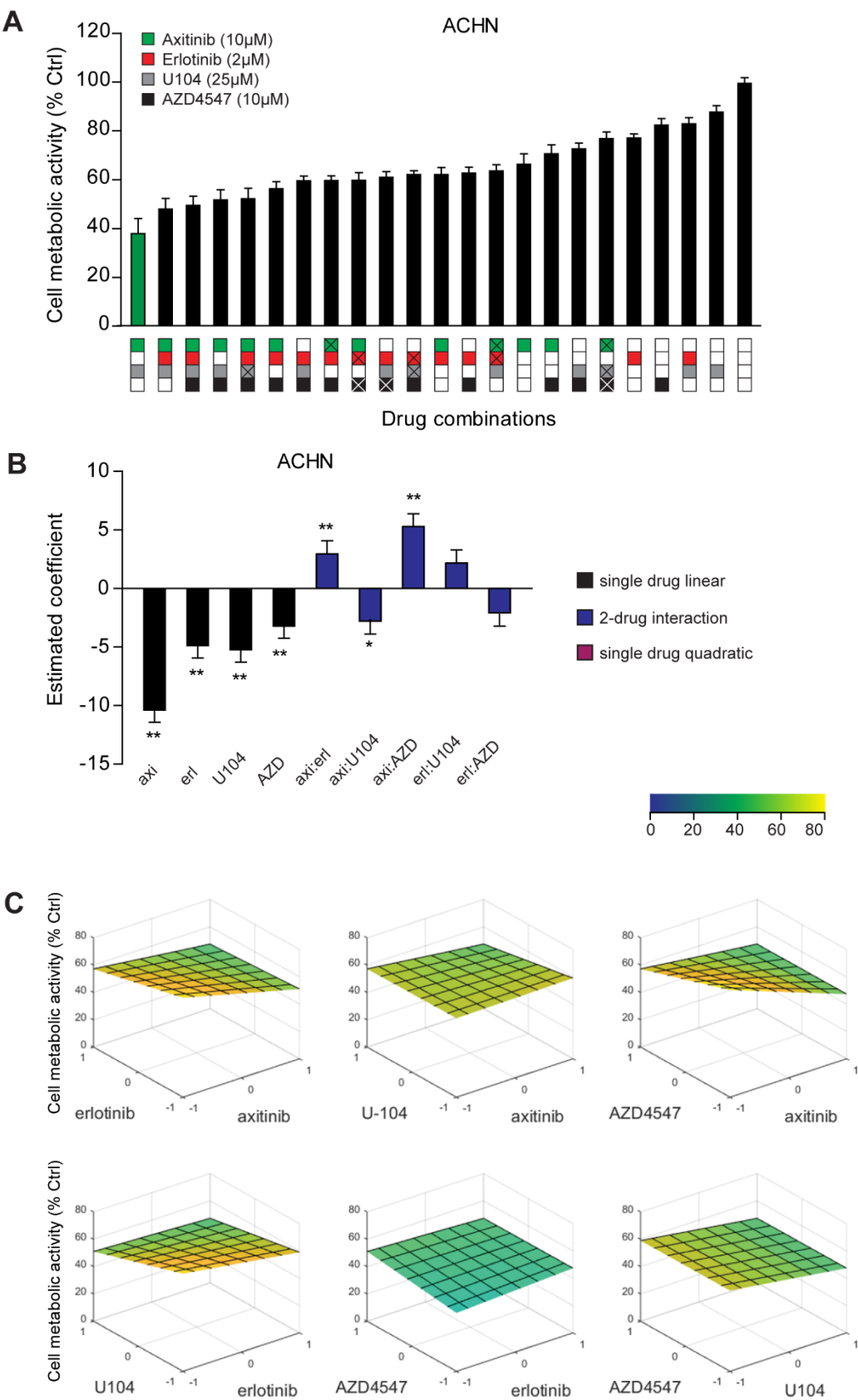




Caki-1







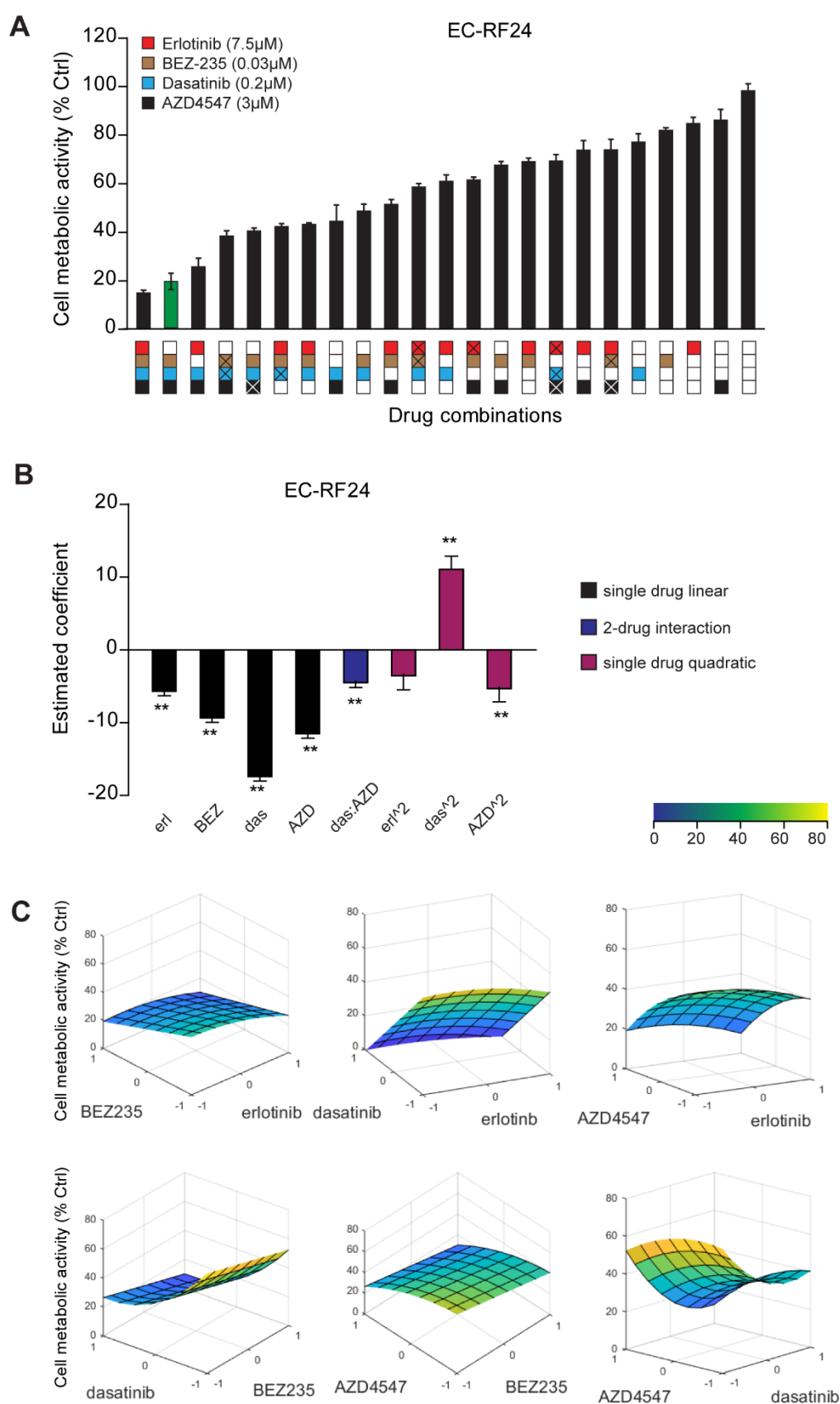


**Figure S1.2.1–6.** Screening for optimized drug combinations. Data are presented for all RCC lines and EC-RF24. (A) Efficacy of the tested drug combinations in search 3. Colored squares below the Y-axis denote drug combinations, with complete fills representing the indicated ( $IC_{20}$ ) concentrations and fills with “X” represent half of the drug concentration. White squares indicate absence of the drug. In

green the ODC (with a maximum of 3 drugs out of 4) is indicated. Experiments (N = 2) were performed in triplicate and mean  $\pm$  SEM are shown. (B) Coefficients from the second order linear regression analysis applied to search 3, composed of the final 4 drugs remaining in the screen and leading to the selection of the ODC. Modeling was based on the data presented in (A). Negative values for single drug linear effects indicate that increasing the dose of that drug increases the inhibition of cell metabolic activity. Negative two-drug interaction values denote synergy, whereas positive values indicate antagonism. Quadratic single drug interactions are a measure of sensitivity to dose changes. C) Response surfaces modelling the interactions between two drugs and their effect on cell metabolic activity while other compounds are held at a constant dose. On the x-axis 1= highest concentration, 0 = lower concentration, -1 = no drug added, and the remaining cell metabolic activity (y-axis) is color coded.

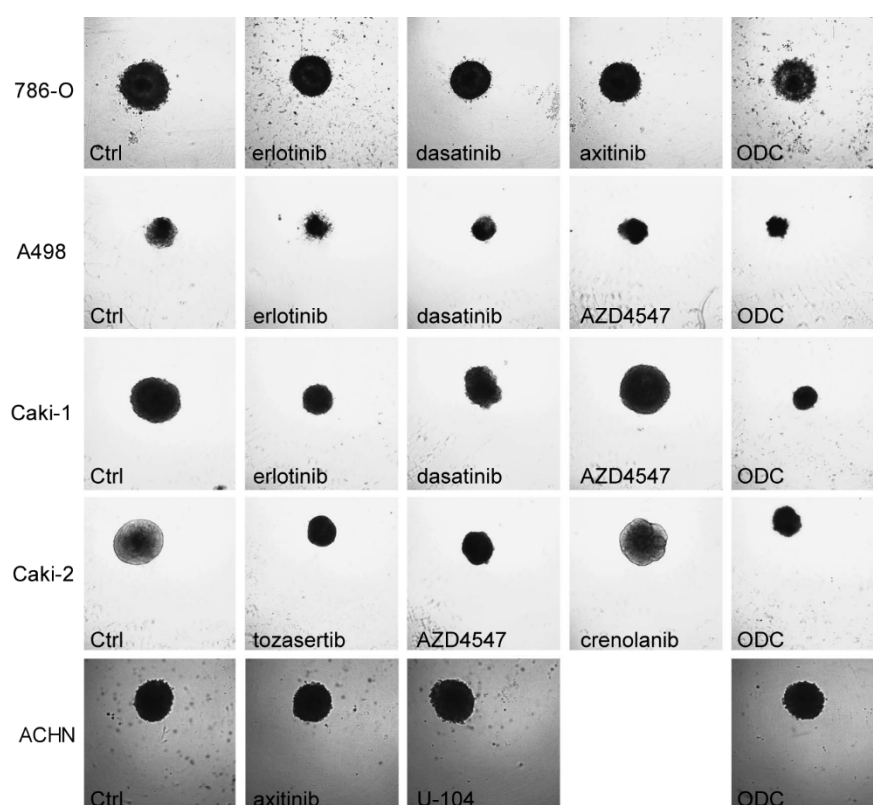


**Figure S1.3.1.** Spheroid morphology after drug treatment. Heterotypic spheroids consisting of a 1:3 mixture of fibroblasts and RCC, supplemented with 10% HUVEC, were treated with either ODC or monotherapy for 72 h before analysis. Due to cell line specific morphology, size was noted not to accurately correlate with metabolic activity (shown in Figure 1).

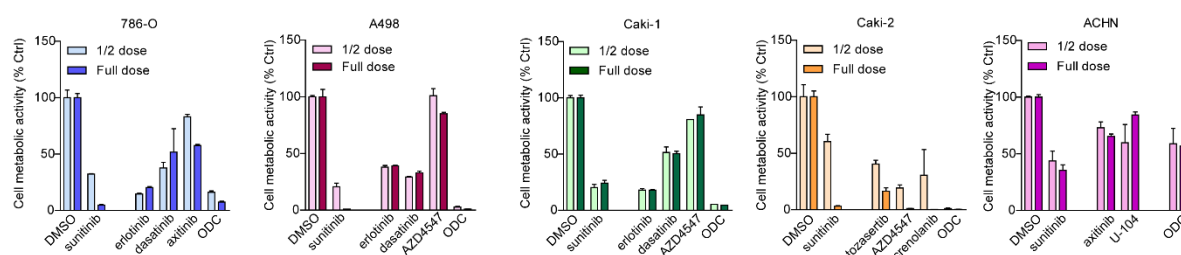


**Figure S1.3.2.** Dose sensitivity in 3D mono- and coculture systems. Homotypic spheroids were formed from RCC lines only and were treated with monotherapies and ODC either at half or at full dose. Similar inhibition is seen with the majority of cell lines and drugs. Dose-sensitivity is only evident in Caki-2 where reducing the dose of the monotherapies considerably impacts the response. However, the ODC effect is apparently not affected by halving the doses of the individual drugs. Experiments (N = 3) were performed in triplicate and mean  $\pm$  SEM are shown.

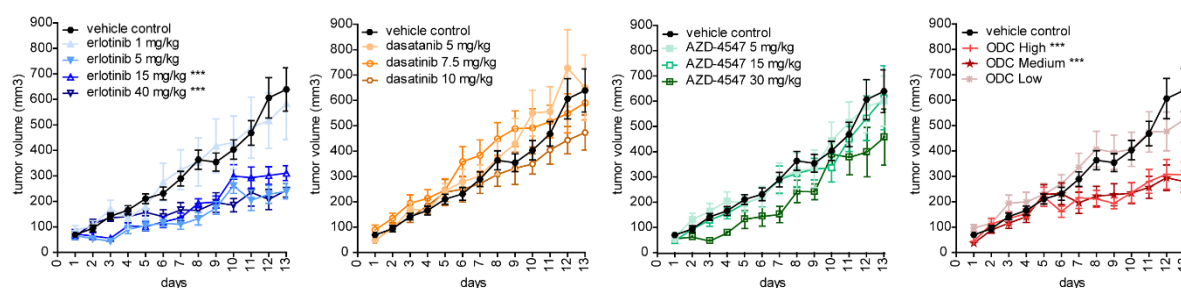


**Figure S1.3.3.** Monotherapies and combinations of drugs in Caki-1 xenografts in mice. Caki-1 tumor volume growth curves of subcutaneous tumor xenografts treated for 13 days with vehicle control, single drugs and drug combinations at various doses in N = 2 independent experiments. Error bars represent the SEM. \*\*\* $p < 0.001$  shown in the graph legend represents the comparison with the vehicle control at day 13 as determined by a two-way ANOVA with post-hoc Dunnett's multiple comparisons test. All erlotinib doses tested were already highly effective in vivo. Doses between 5–40 mg/kg, corresponding to 0.26–2  $\mu\text{M}$  *in vitro* inhibited tumor growth by over 60%. For dasatinib and AZD4547, s-FSC-based doses showed no significant tumor growth inhibition. The *in vivo* dominance of erlotinib was further confirmed in the drug combinations where the activity was driven mostly by erlotinib. However, together, the ODCs show potent effects *in vitro* and *in vivo*.

## Supplement 2: Characterization of ODC effects in RCC

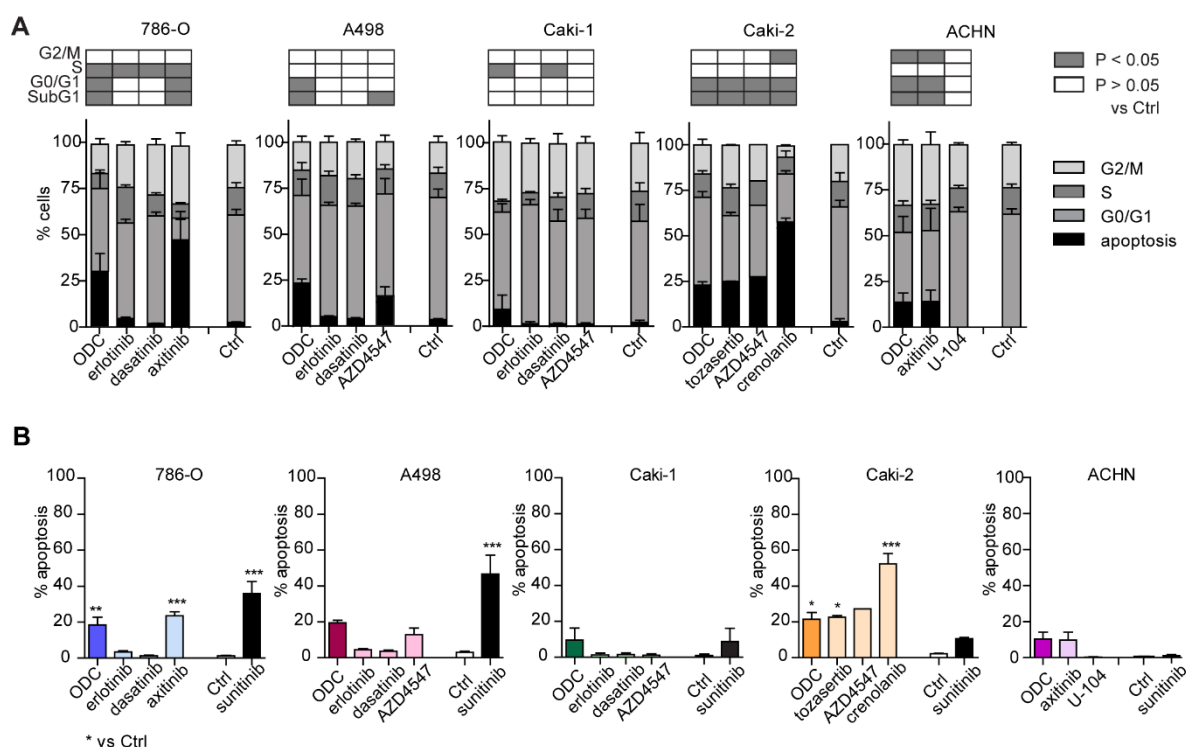


**Figure S2.1.** Effects of ODC on cell cycle profile. A) RCC were treated with monotherapies or ODC for 72 h and subject to flow-cytometry based cell cycle analysis by propidium iodide staining for cellular DNA content. In general, ODC treatment induced apoptosis in the cell lines. Most monotherapies do not affect the distribution of the different cell cycle phases as compared to control, with the exception of axitinib and crenolanib that seem to induce apoptosis. Significant changes in the different phases are indicated at the top of the graph. B) For a direct comparison, the sub-G1 fraction was classified as apoptotic fraction. In these experiments, sunitinib (10  $\mu$ M) was used as a positive control as this compound is among first-line treatments for RCC. ccRCC lines showed apoptosis induction by sunitinib at comparable levels to ODC, whereas the papillary RCC lines were totally insensitive. Of note, crenolanib alone clearly induced cell death in Caki-2, however in combination with other drugs this effect is reduced. N = 5 independent experiments were performed and results shown represent mean  $\pm$  SEM.

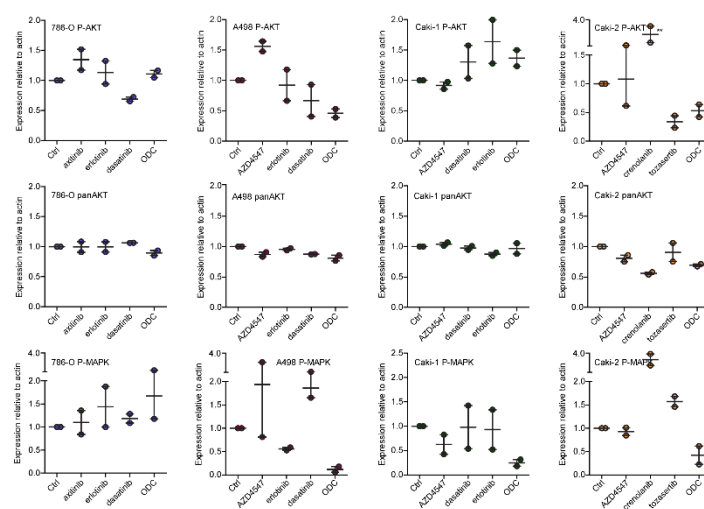


**Figure S2.2.** Mechanism of action of drug combinations. Quantification of western blots. Bands shown in Figure 2 were quantified densitometrically. Monotherapies tend to have only limited effect on phosphorylation of the analyzed kinases, whereas the ODC is most effective in inhibiting MAPK (ERK1/2) phosphorylation. A notable exception is 786-O where the ODC does not impact the phosphorylation of AKT and MAPK. Duplicate experiments were performed.

### Supplement 3: Phosphoproteomics analysis of RCC lines

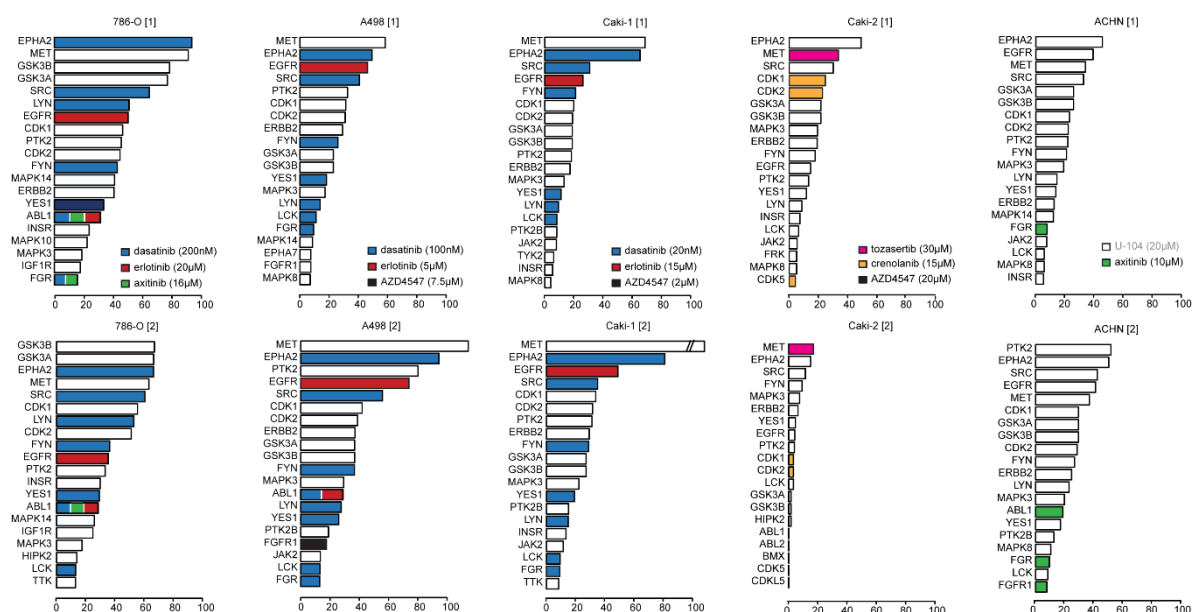


**Figure S3.1.1.** Duplicate INKA analysis of RCC lines. INKA ranking plots of duplicate samples for all RCC lines. Kinases targeted by drugs in the ODC are color-coded according to their respective legends.



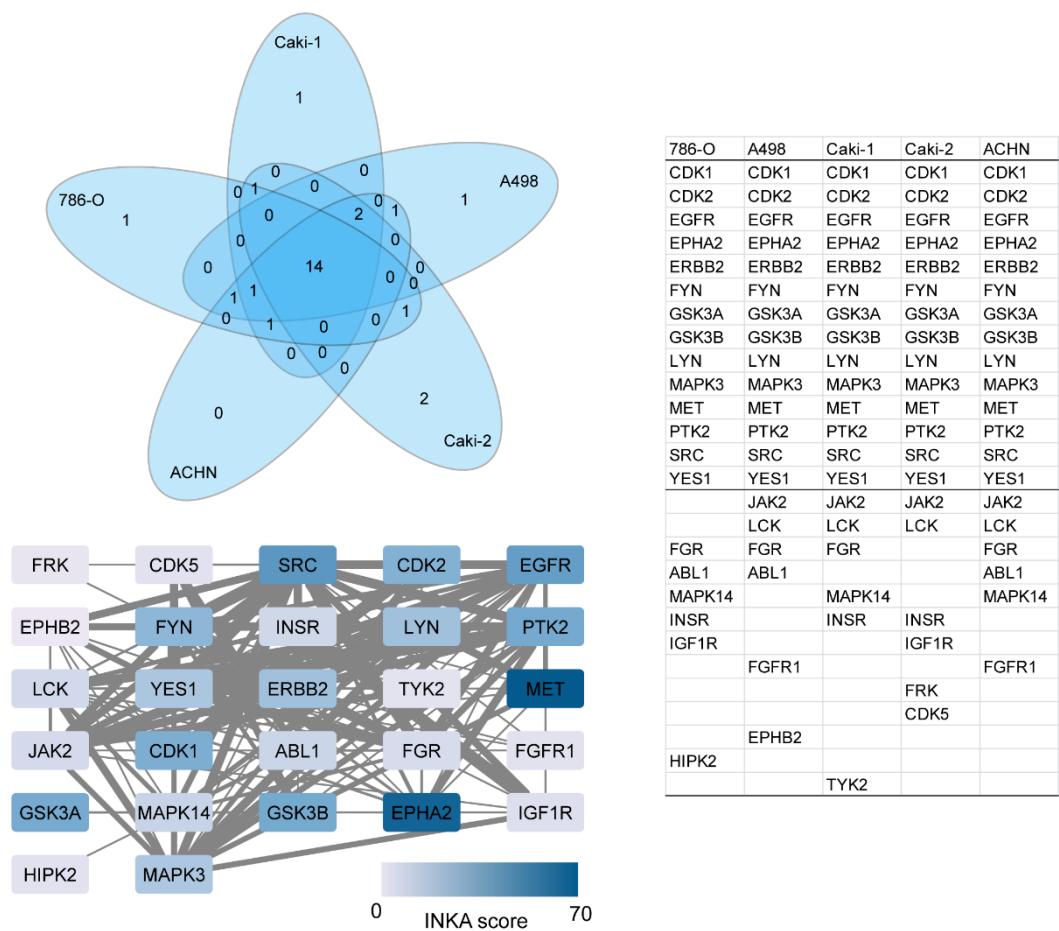


**Figure S3.1.2.** Overlap of top 20 INKA kinases in 5 RCC lines. Top 20 kinases from the INKA analysis were derived from the average scores per cell line. Venn diagram shows that 14 are commonly present in this top 20, and that 8 more are present in the top 20 of 2 or more cell lines. Protein-protein interaction analysis shows the close interconnectivity of these kinases.

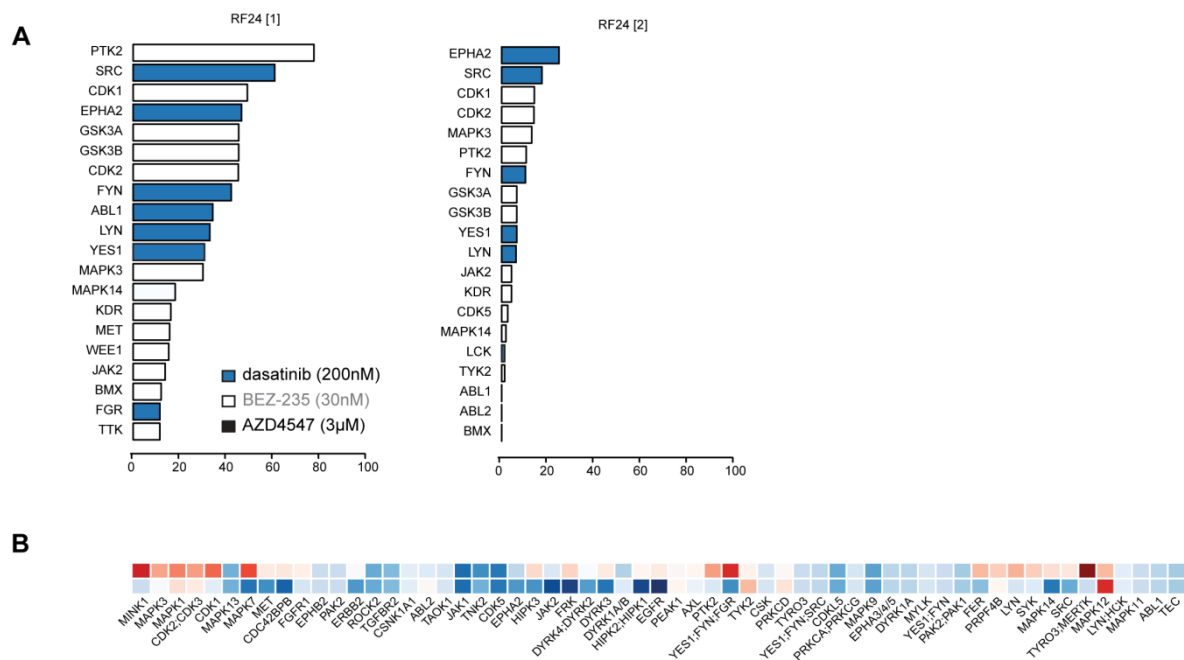
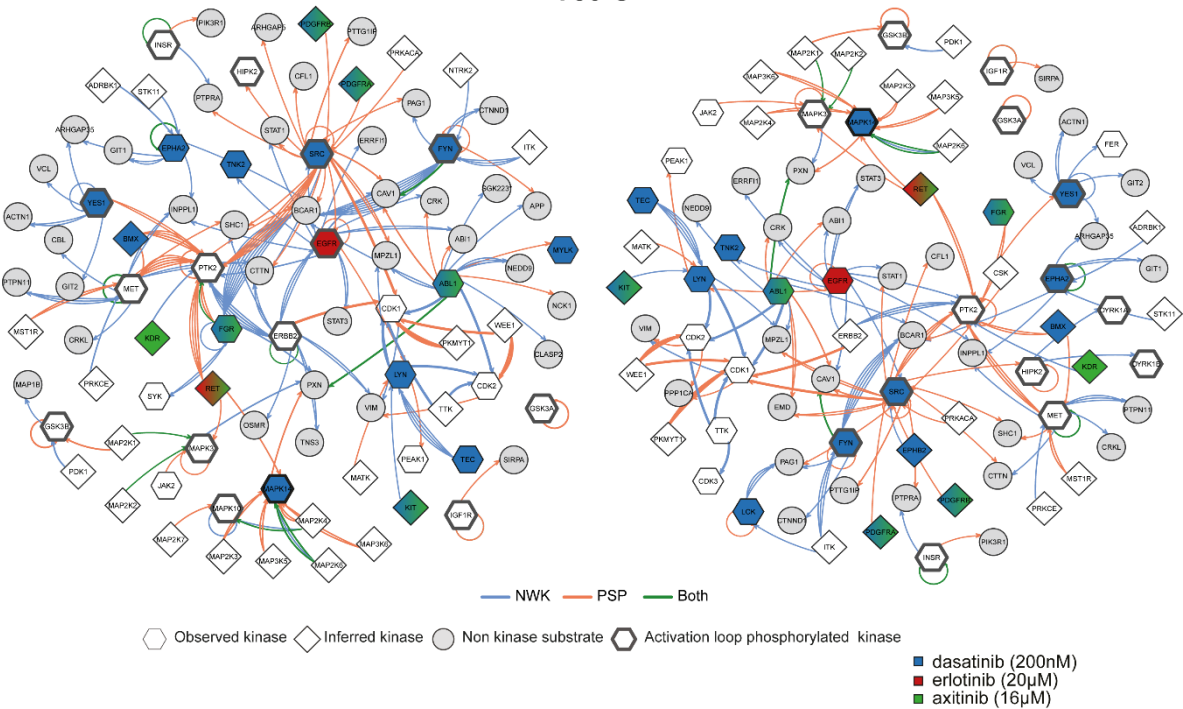


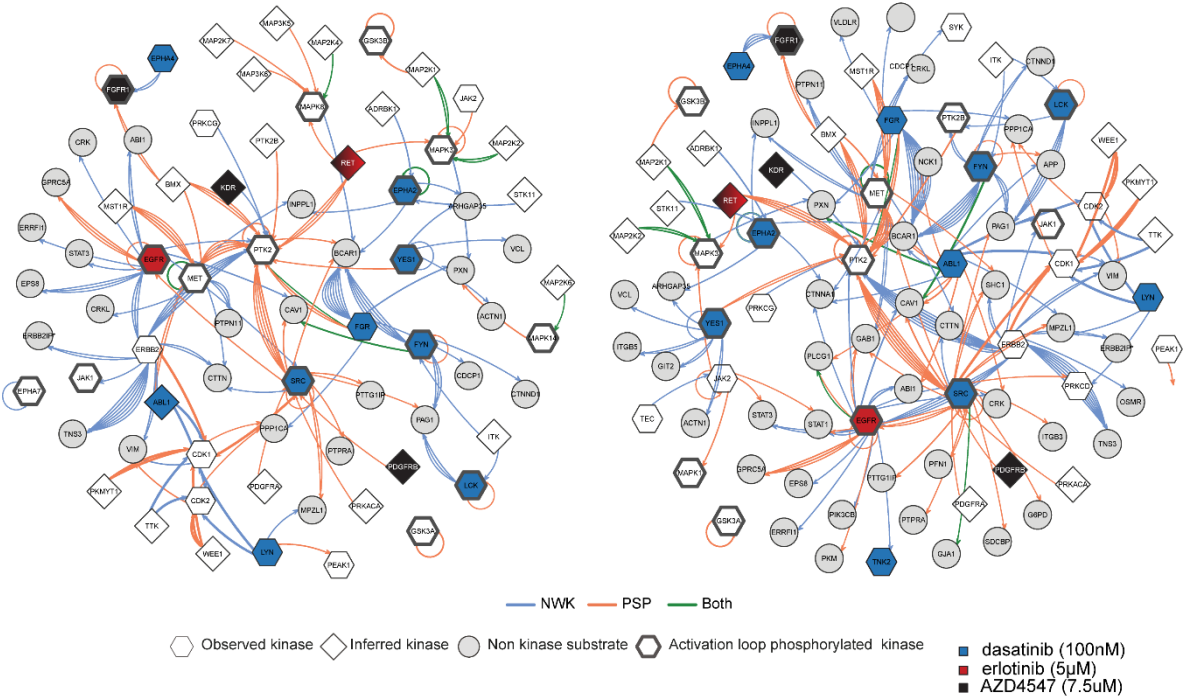
Figure S3.1.3  
Figure S3.1.3 Phosphoproteomics analysis of EC-RF24

A) INKA ranking plots of duplicate samples of untreated EC-RF24 cells. Drug targets in the top 20 are color-coded. B) Phosphokinase expression levels, expressed in relation to those in RCC lines shown in Figure 3.

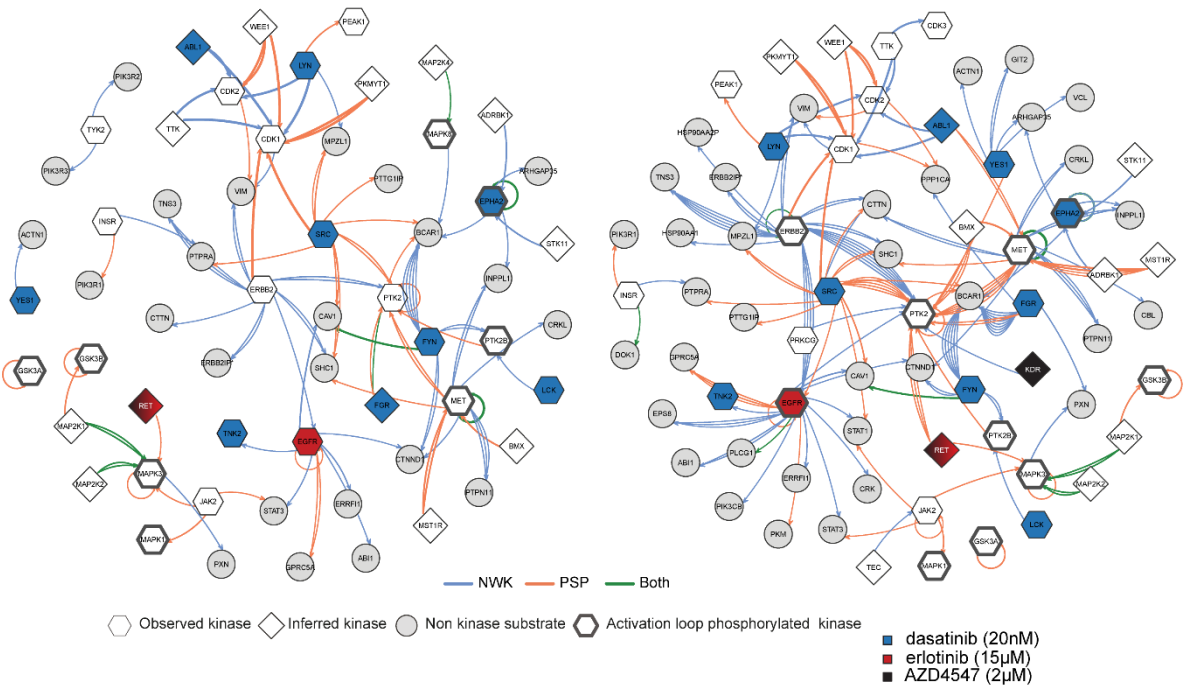
786-O



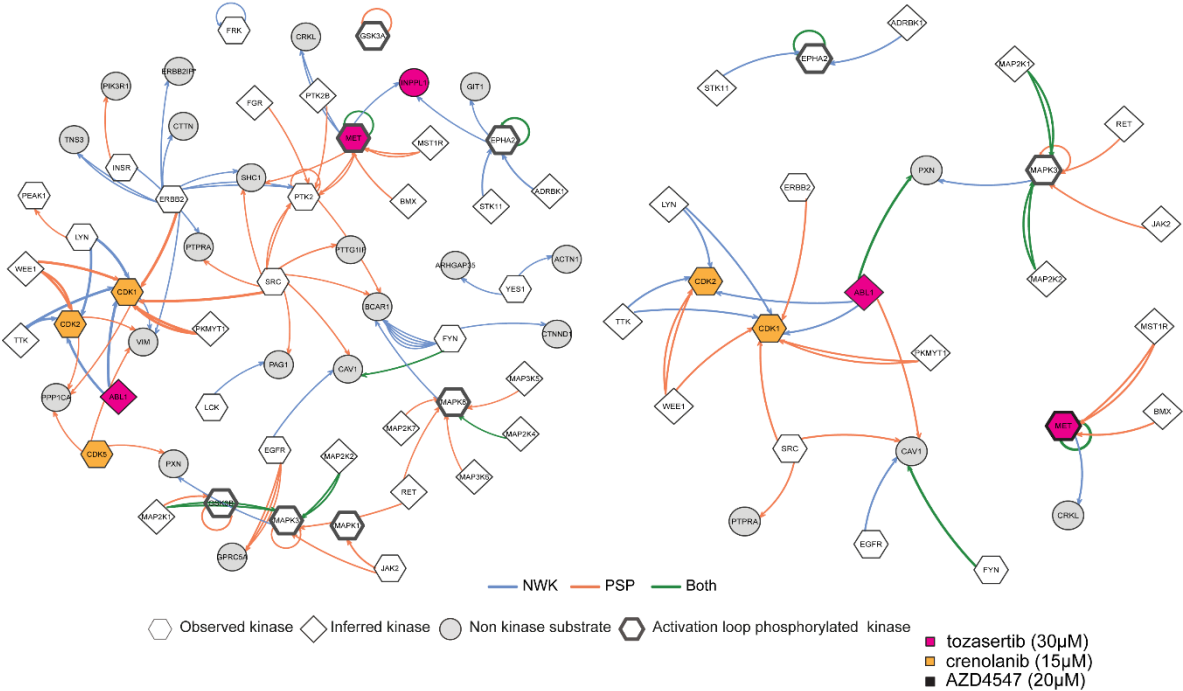
A498



Caki-1



Caki-2



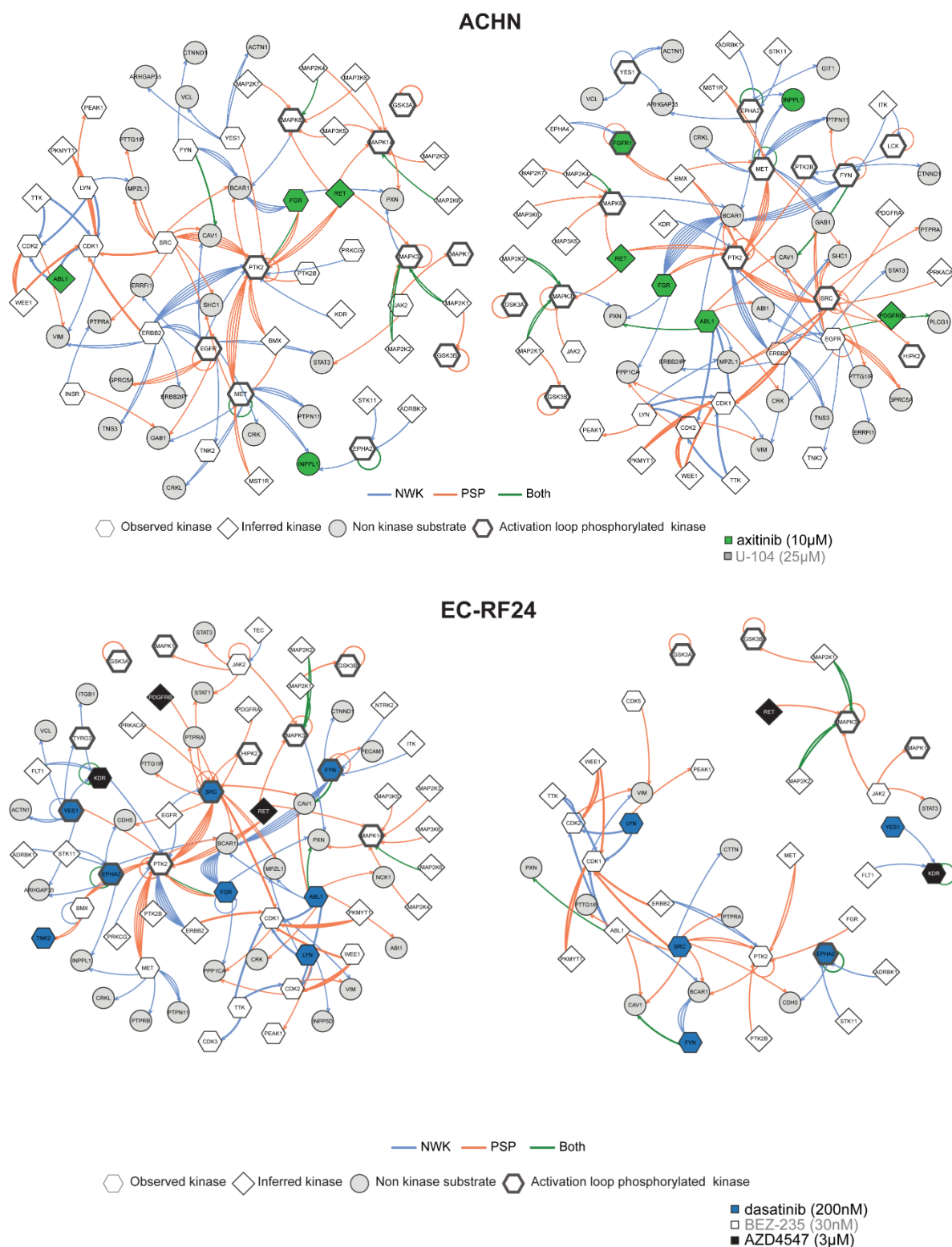


Figure S3.2.6

**Figure S3.2.1–6.** INKA network plots of RCC lines **ACHN** and **EC-RF24**. Kinase-substrate relationship of top 20 INKA kinases and their observed substrates in duplicate samples. Nodes are color-coded for targeting by drugs in the ODC. Drug targets are shaped according to INKA evidence. Nodes are depicted as a hexagon (observed kinases, identified through one or more phosphopeptides), a pentagon (inferred kinases lacking direct observation, but linked to phosphorylation of one or more observed phosphopeptides), or as a circle (non-kinase substrates). Edge widths correlate with the associated substrate site “phosphosignal”, and edge colors indicate the analysis on which the kinase–substrate relationship was based (orange: PSP, blue: NWK, green: both).



## Supplement 4: A common drug combination for RCC lines

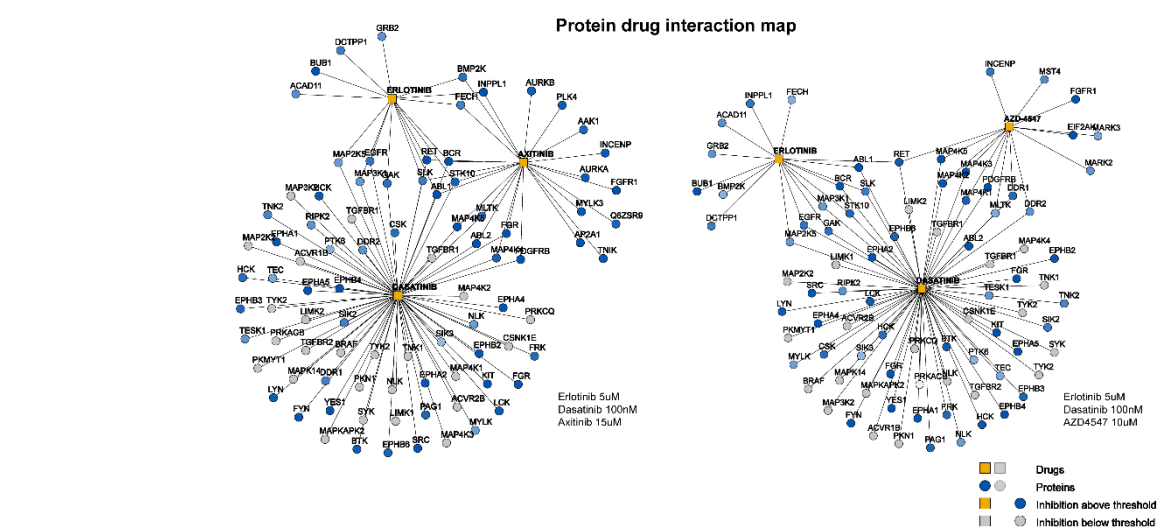
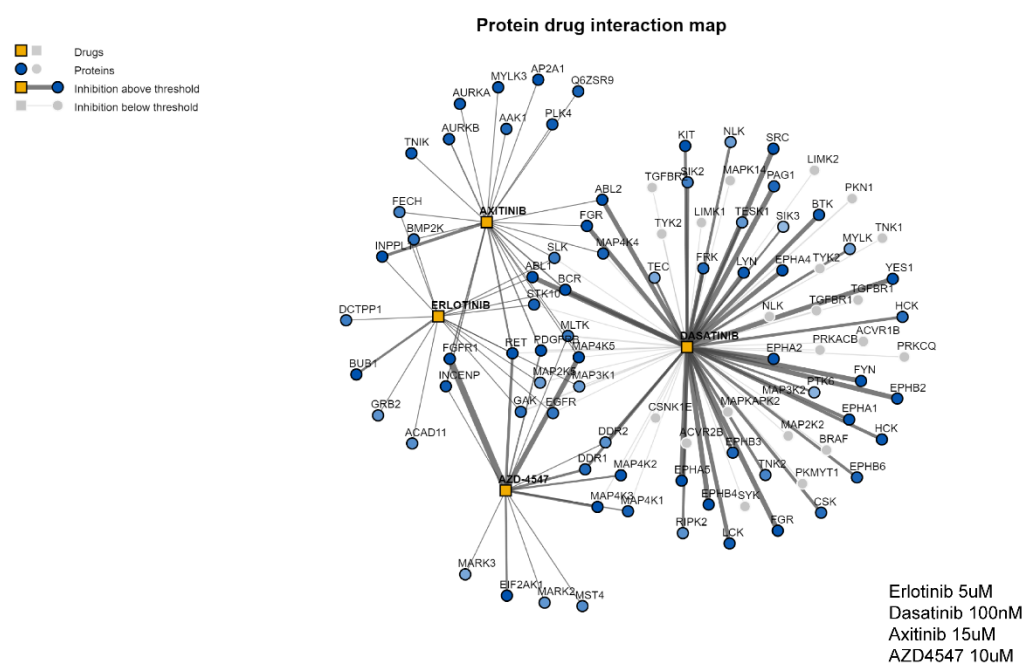


Figure S4.1.1



**Figure S4.1.1–2.** Protein drug interaction maps. Protein drug interaction maps ([www.proteomicsdb.org](http://www.proteomicsdb.org)) using the median concentrations of the 4 drugs presented in Table S4.1. Combinations of 3 and 4 drugs are shown, and reveal a number of multitargeted kinases. Protein kinase targets (nodes) exceeding default effective inhibition >33% are colored in blue and have dark grey edges. Thickness of the edges is proportional to the reported EC50 of the drug-kinase interaction.

## Supplement 5: Phosphokinase alterations in 786-O after ODC



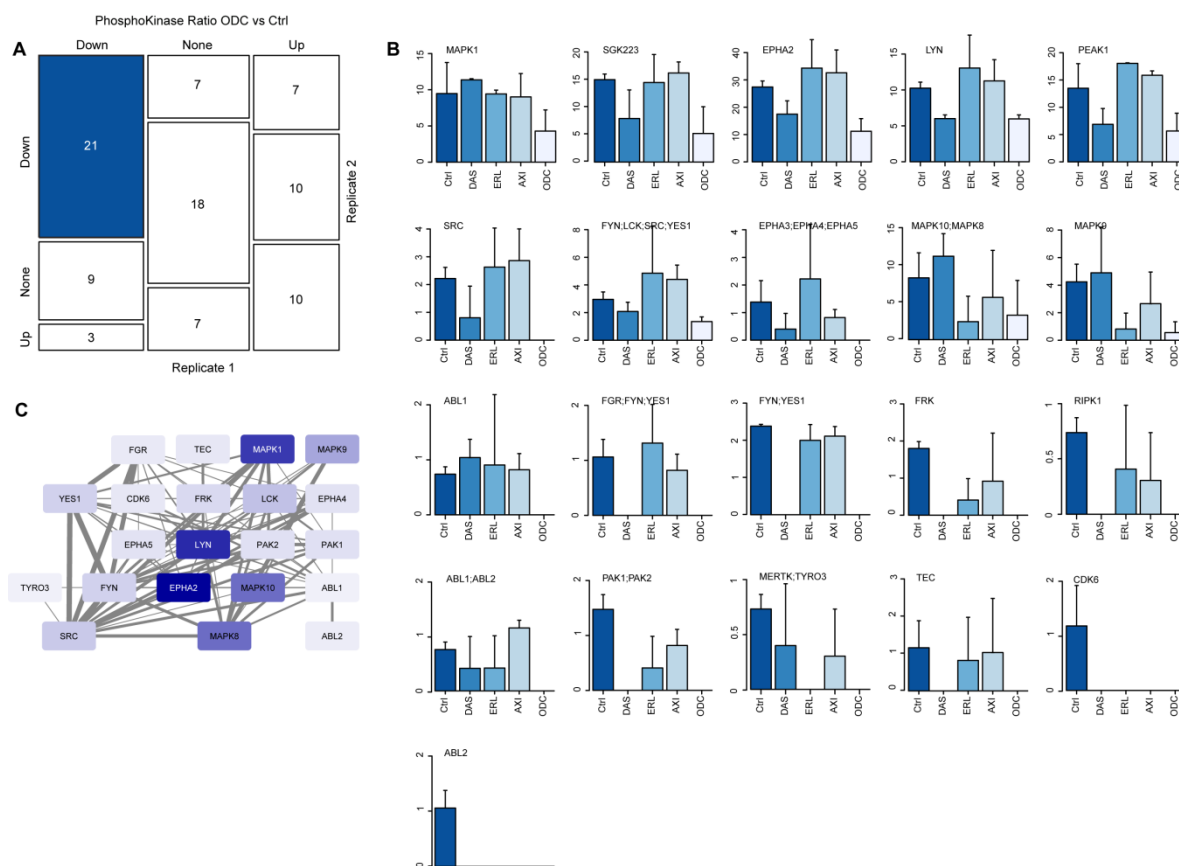


**Figure S5.1.1.** Phosphokinases (pTyr) downregulated after ODC. **(A)** Phosphoproteomics analysis was performed on pTyr-IP'ed proteins from 786-O treated with the different monotherapies (dasatinib 150nM, erlotinib 10uM, axitinib 7.5uM), ODC, or left untreated for 2 hours. Phosphopeptides were assembled to phosphogenes and subsequently phosphorylated kinases as described in the materials and methods section. Normalized spectral counts were used as quantifiers and kinases showing >1.6 fold downregulation following ODC were counted in the replicate experiments. 21 phosphokinases were consistently downregulated. **(B)** Average normalized spectral counts of phosphorylated kinases consistently inhibited by the ODC. Due to ambiguity in phosphopeptide identification, multiple protein identifiers are mentioned for several of the hits. Most notable are the MAPK family, SRC family, ABL family and EPHA family kinases. **(C)** Protein-protein interaction network of the ODC inhibited kinases shows intricate interactions between them. Color intensity of the nodes is proportional to expression level.



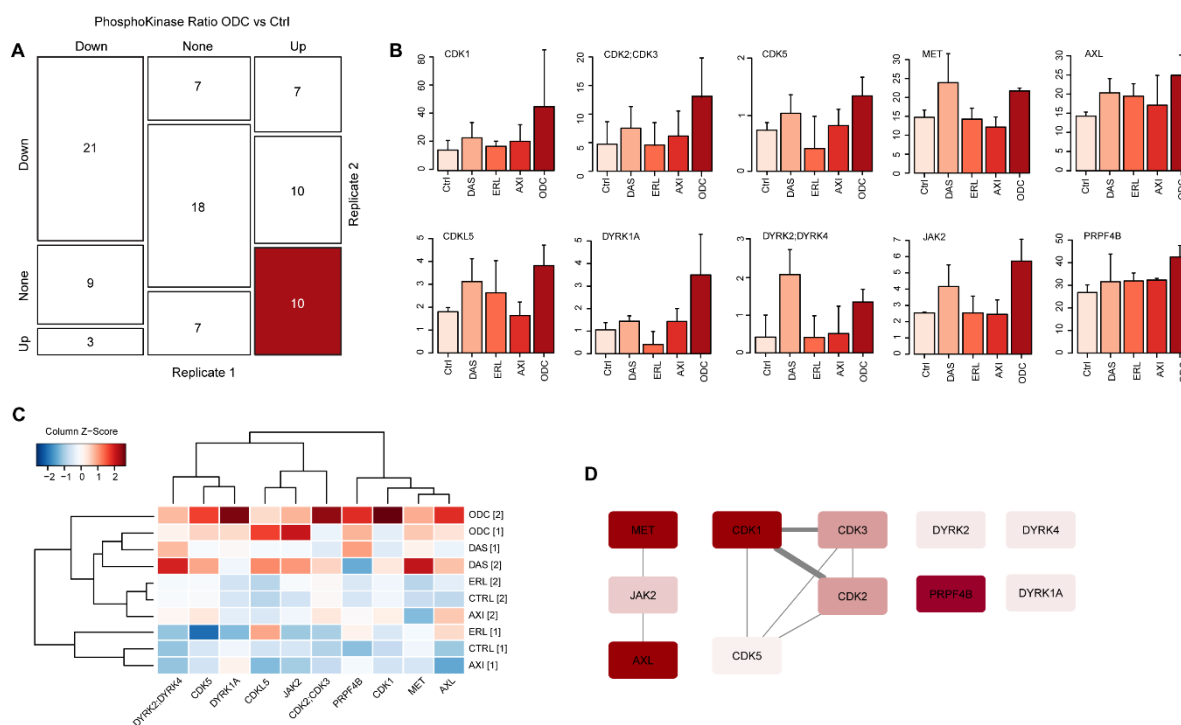


**Figure S5.1.2.** Phosphokinases (pTyr) upregulated after ODC. (A) Phosphoproteomics analysis was performed on pTyr-IP'ed proteins from 786-O treated with the different monotherapies (dasatinib 150nM, erlotinib 10uM, axitinib 7.5uM), ODC, or left untreated for 2 hours. Phosphopeptides were assembled to phosphogenes and subsequently phosphorylated kinases as described in the materials and methods section. Normalized spectral counts were used as quantifiers and kinases showing >1.3 fold upregulation following ODC were counted in the replicate experiments. 10 phosphokinases were consistently upregulated. (B) Average normalized spectral counts of phosphorylated kinases consistently induced by the ODC. Due to ambiguity in phosphopeptide identification, multiple protein identifiers are mentioned for several of the hits. Most notable are the CDK family and DYRK family kinases. Induction of putative resistance mediating kinases (JAK, MET, AXL) is also noted. (C) Heatmap of induced kinases, showing that kinase alterations are dominantly mediated by dasatinib. (D) Protein-protein interaction network of the ODC induced kinases. The MET-JAK2-AXL axis showed significant enrichment for the KEGG pathway “EGFR tyrosine kinase inhibitor resistance” (p=0.00079). Color intensity of the nodes is proportional to expression level.

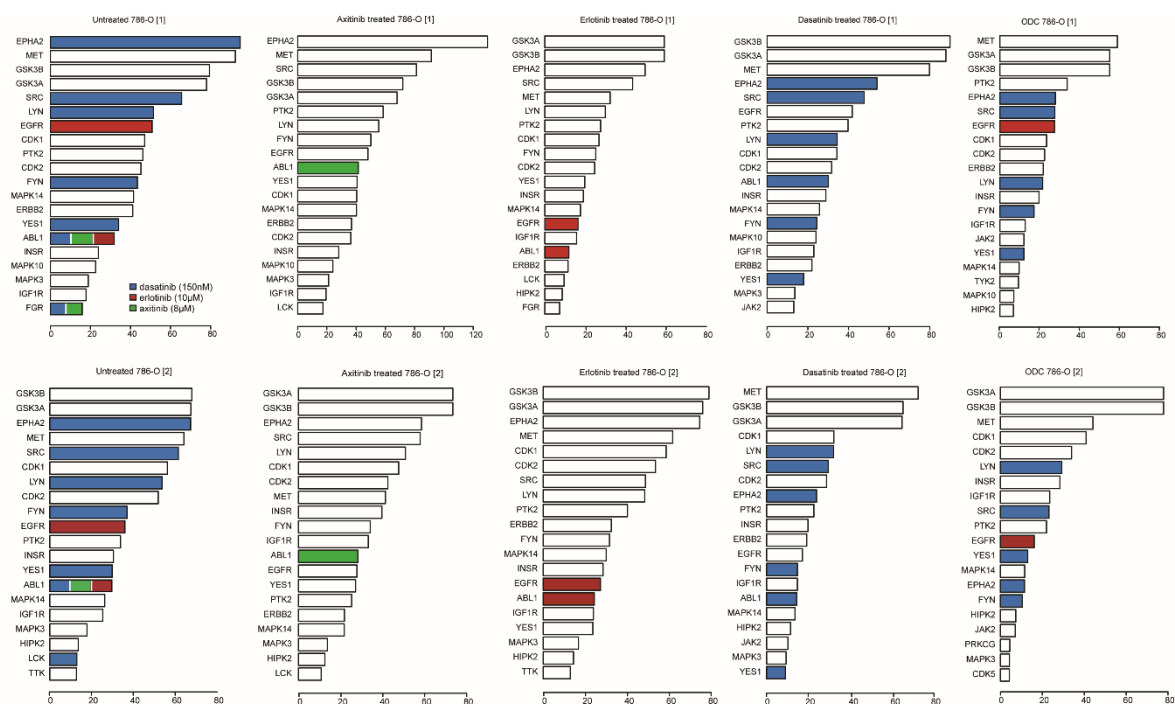
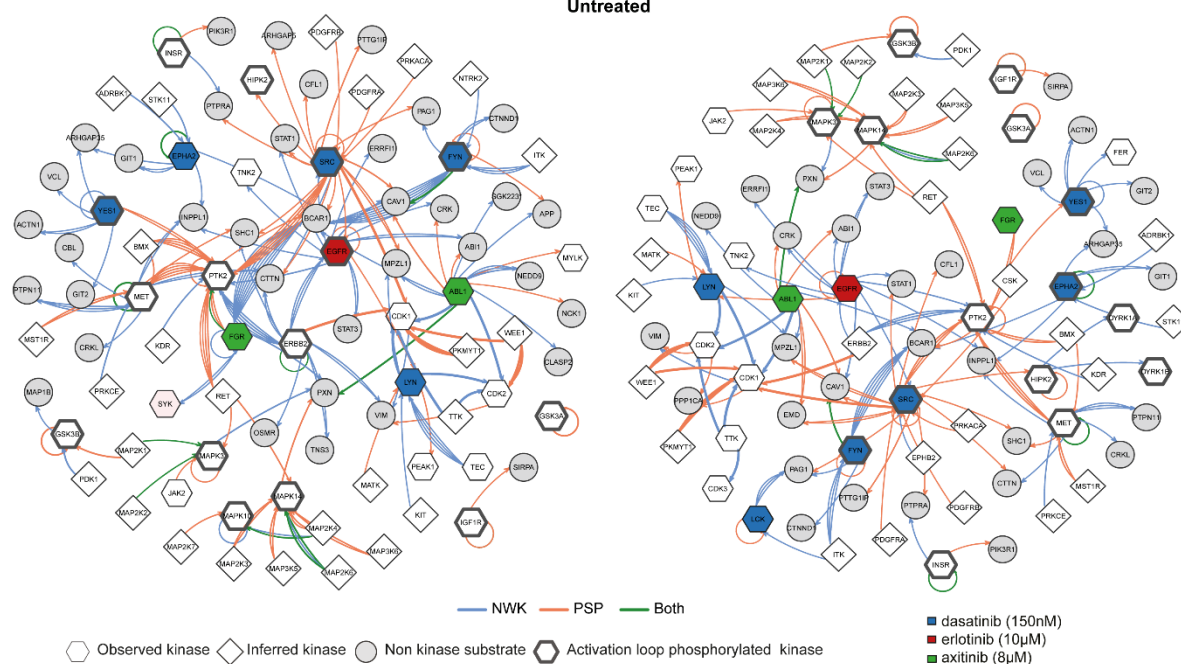
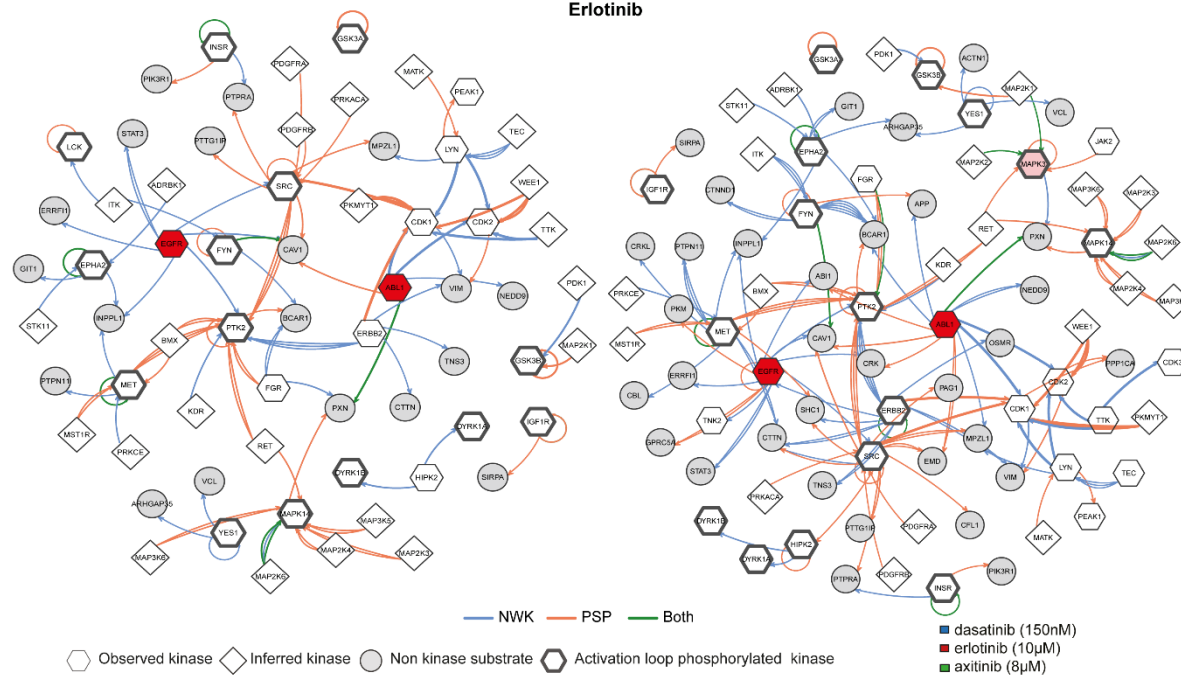


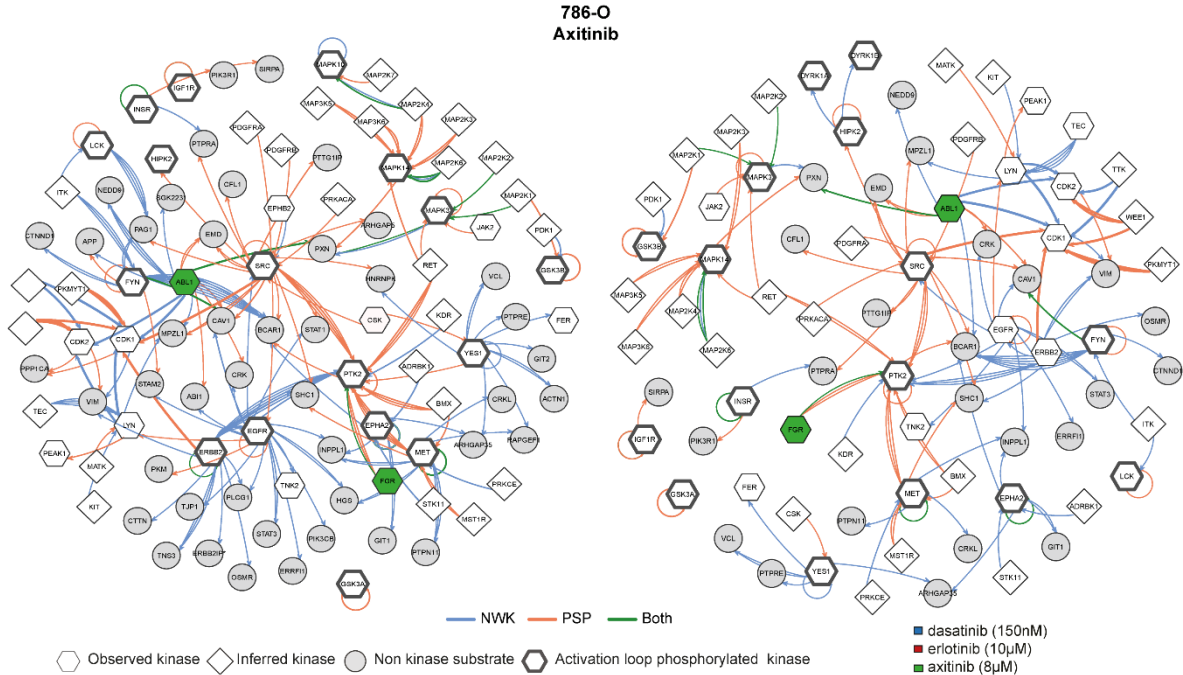
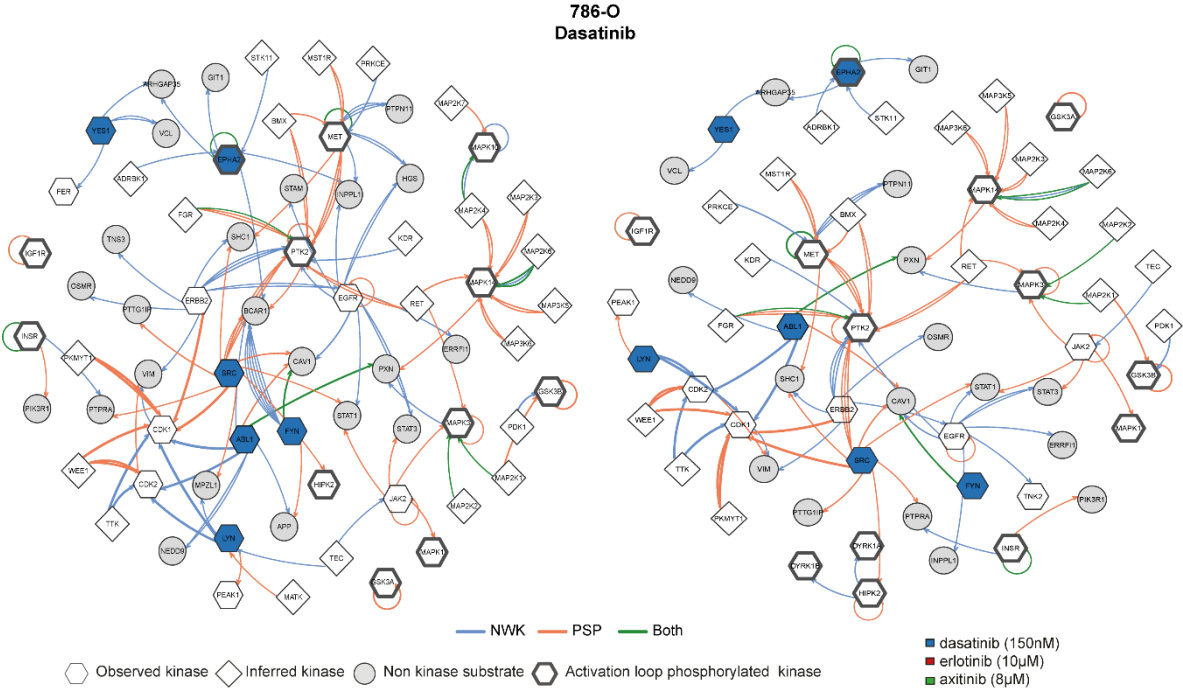
**Figure S5.2.** INKA profiles after monotherapies and ODC in 786-O. INKA ranking plots of duplicate samples for treated and untreated 786-O. Kinases targeted by drugs are color-coded according to their respective legends. For untreated 786-O all drug targets are indicated in their respective colors. These plots allow for the relative ranking of kinases before and after treatment.

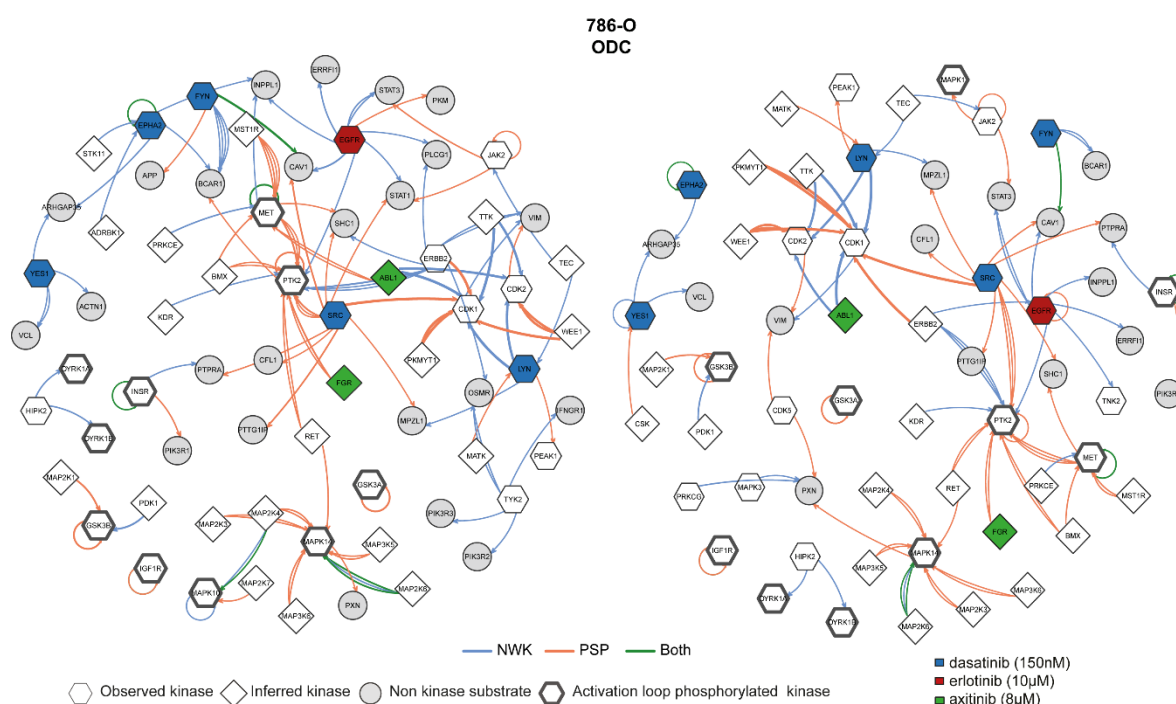
### 786-O Untreated



### 786-O Erlotinib

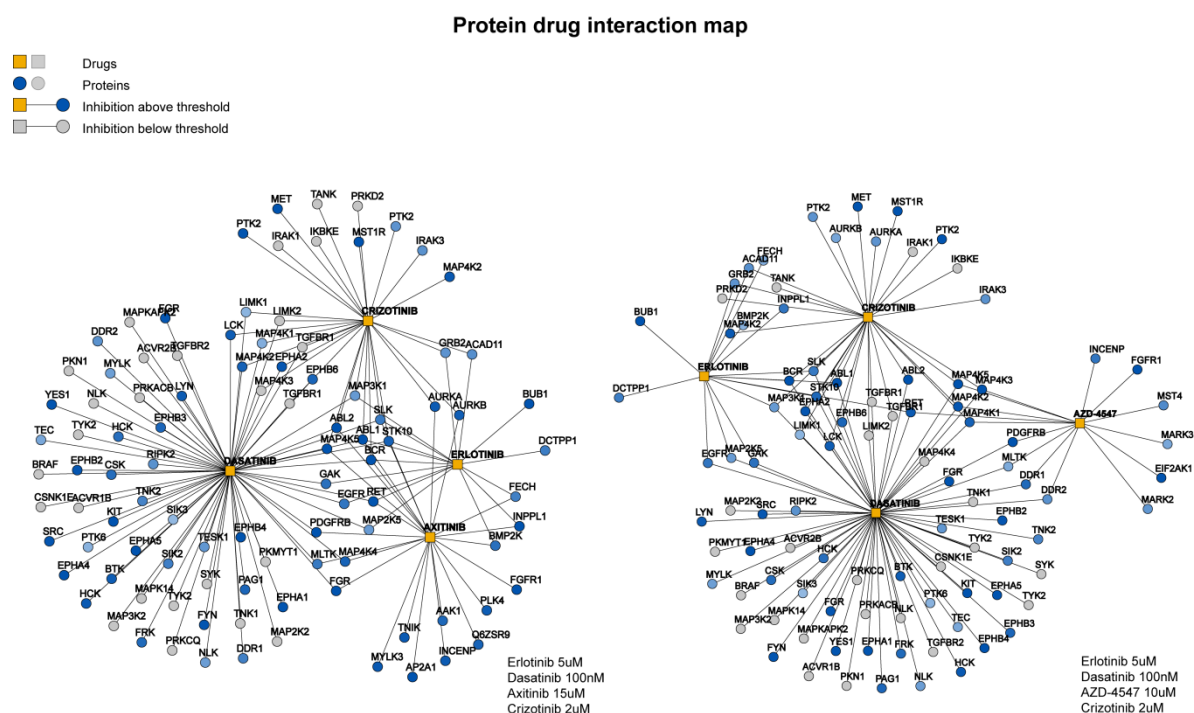






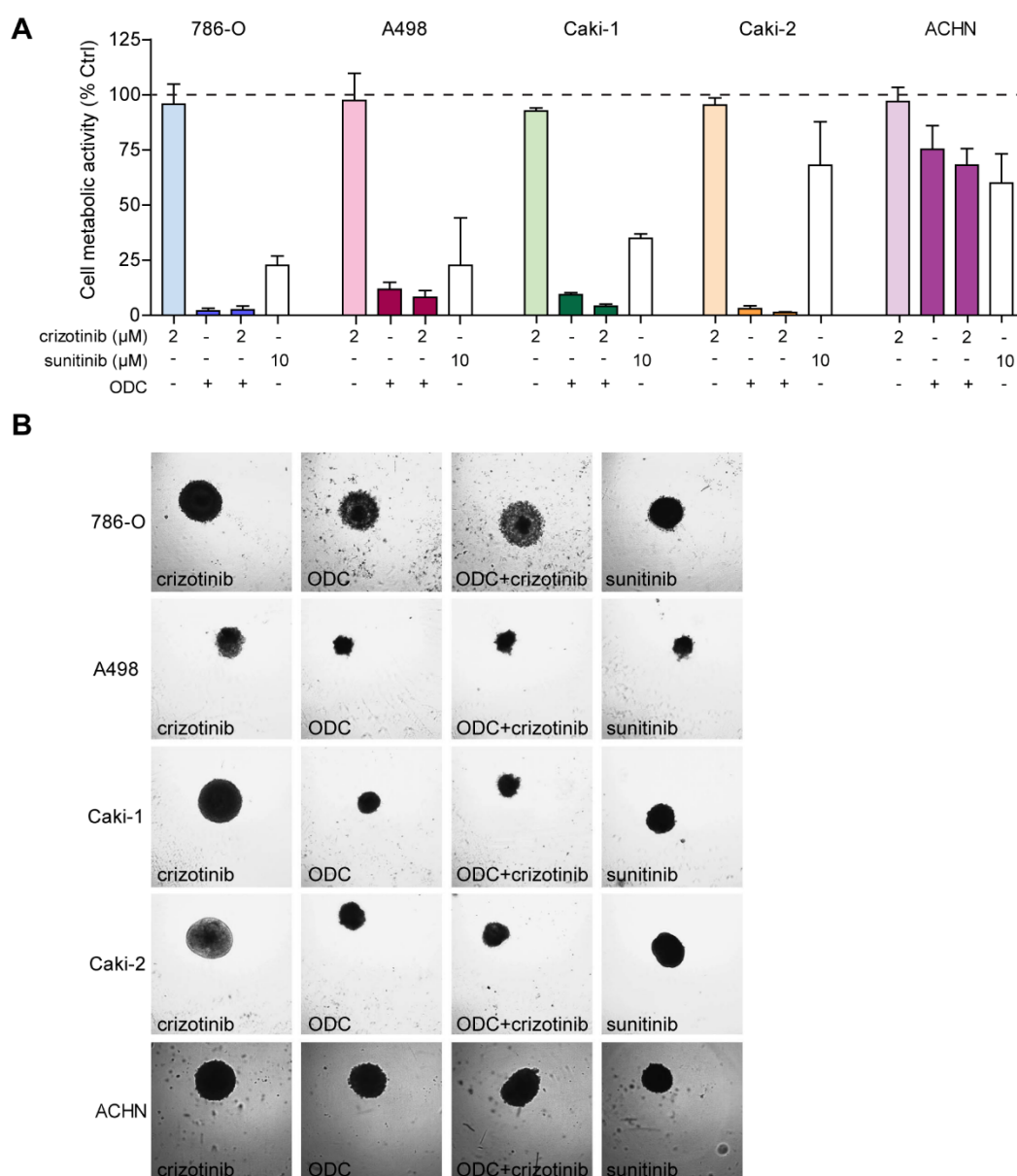
**Figure S5.3.1–5.** INKA network plots of monotherapies and ODC in 786-O. Kinase-substrate relationship of top 20 INKA kinases and their observed substrates in duplicate samples. Nodes are color-coded for targeting by drugs in the ODC. Drug targets are shaped according to INKA evidence. Nodes are depicted as a hexagon (observed kinases, identified through one or more phosphopeptides), a pentagon (inferred kinases lacking direct observation, but linked to phosphorylation of one or more observed phosphopeptides), or as a circle (non-kinase substrates). Edge widths correlate with the associated substrate site “phosphosignal”, and edge colors indicate the analysis on which the kinase–substrate relationship was based (orange: PSP, blue: NWK, green: both).

## Supplement 6: Effects of addition of crizotinib on ODC performance



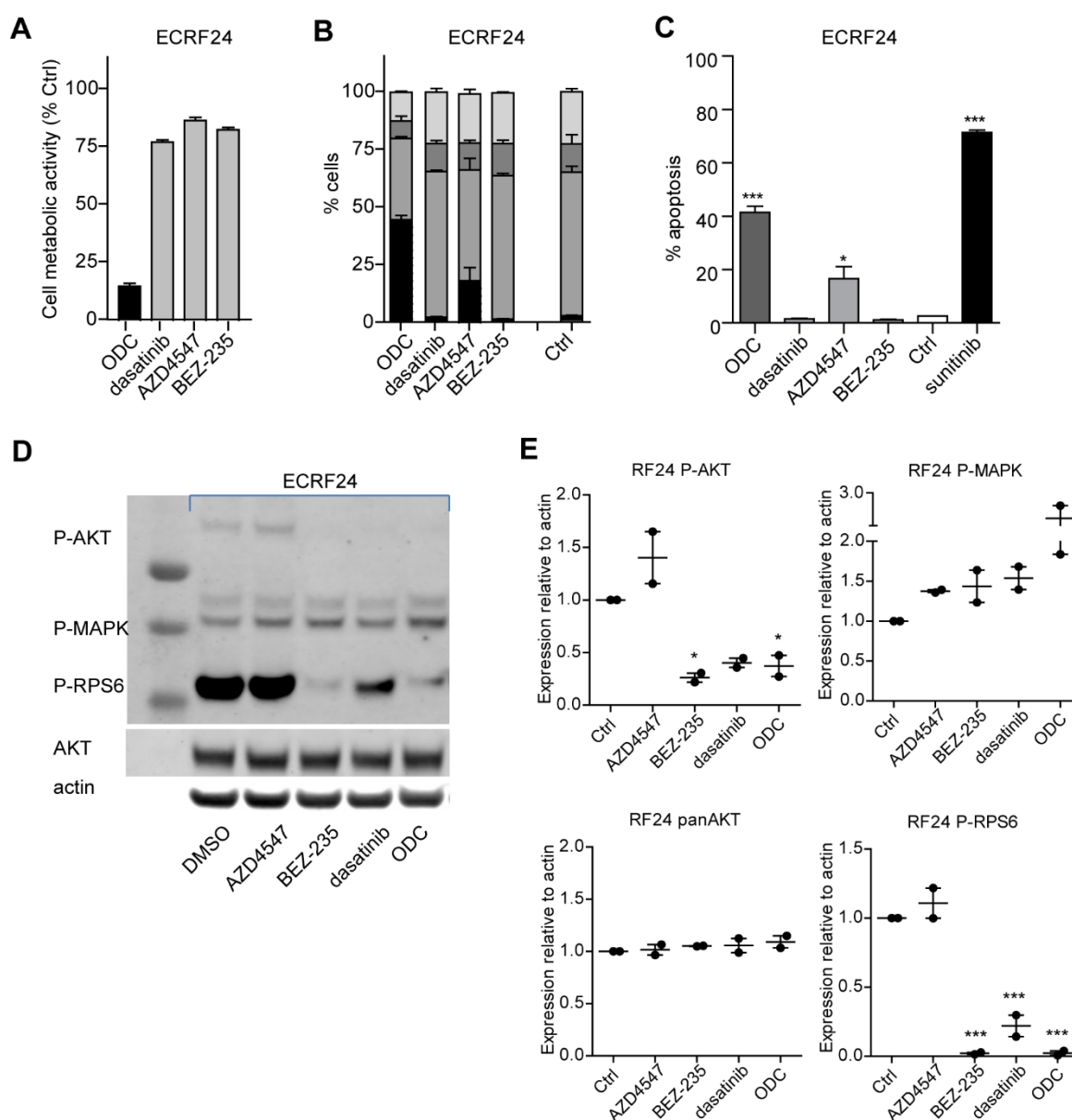
**Figure S6.1.** Protein-drug interaction maps. Protein drug interaction maps ([www.proteomicsdb.org](http://www.proteomicsdb.org)) for the combinations of erlotinib, dasatinib, crizotinib and AZD4547 or axitinib, reveal a number of multitargeted kinases. Protein kinase targets (nodes) exceeding default effective inhibition >33% are colored in blue and have dark grey edges. Thickness of the edges is proportional to the reported EC<sub>50</sub> of the drug-kinase interaction.





**Figure S6.2.** Limited additional effect of crizotinib addition in 3D cultures. (A) 2μM crizotinib was selected for addition to the ODC. Applied as monotherapy, crizotinib displayed <10% inhibitory activity in heterotypic 3D cultures. When added to the original ODC, no further inhibition of cell metabolic activity is observed, as the ODC displayed more potent inhibitory activity in 3D as compared to 2D in vitro assays. Experiments (N = 2–4) were performed in triplicate and mean ± SEM is shown. (B) Representative images of spheroids after treatment.

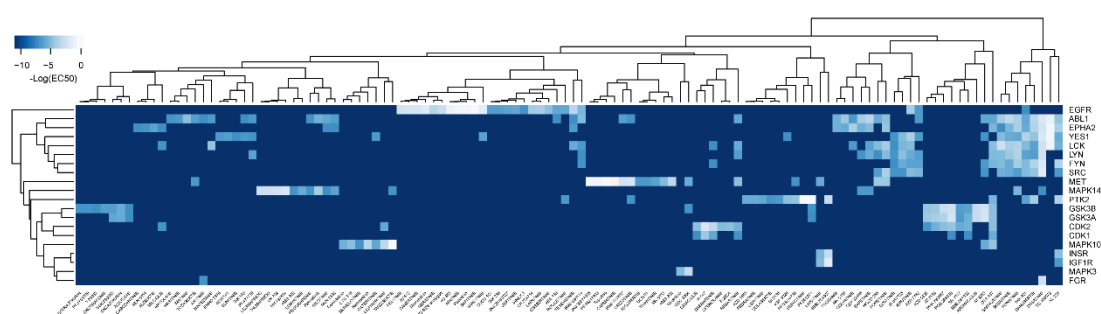
## Supplement 7: Analysis in EC-RF24



**Figure S7.1.** ODC in EC-RF24. (A) Dasatinib, AZD4547 and BEZ-235 were selected as ODC in EC-RF24. Alone, they inhibit cell metabolic activity by <25%, whereas in combination their effect is >85%. N=3 independent experiments were performed and results shown represent mean  $\pm$  SEM. (B,C) Cell cycle analysis (B) and apoptosis analysis (C) reveals an increase in apoptosis after ODC treatment, which is in part mediated by AZD4547. N=2 independent experiments were performed and results shown represent mean  $\pm$  SEM. (D,E) Western blot analysis shows a dominant action of dasatinib and BEZ-235 on phospho-AKT and phospho-RPS6 expression.



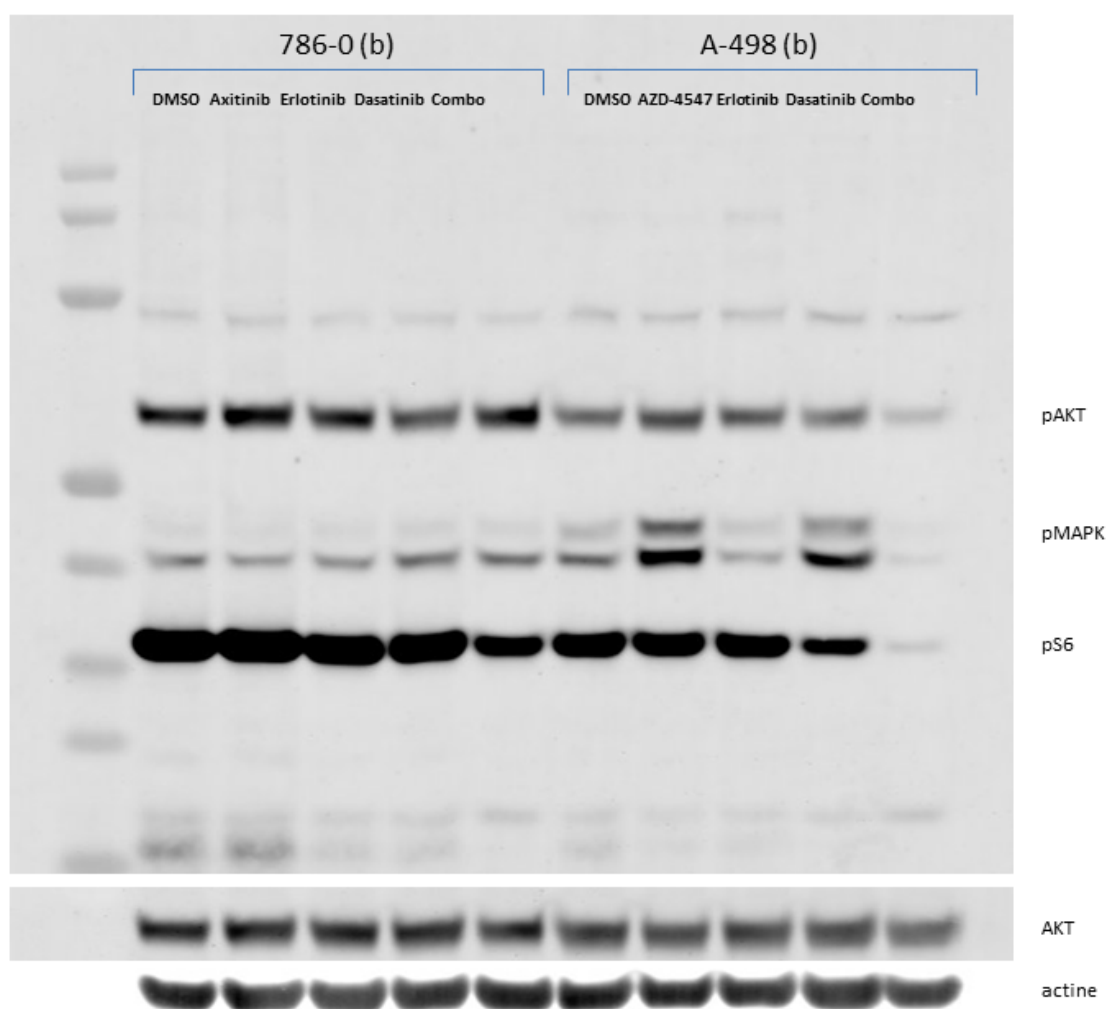
## Supplement 8: Drug-kinase efficacy



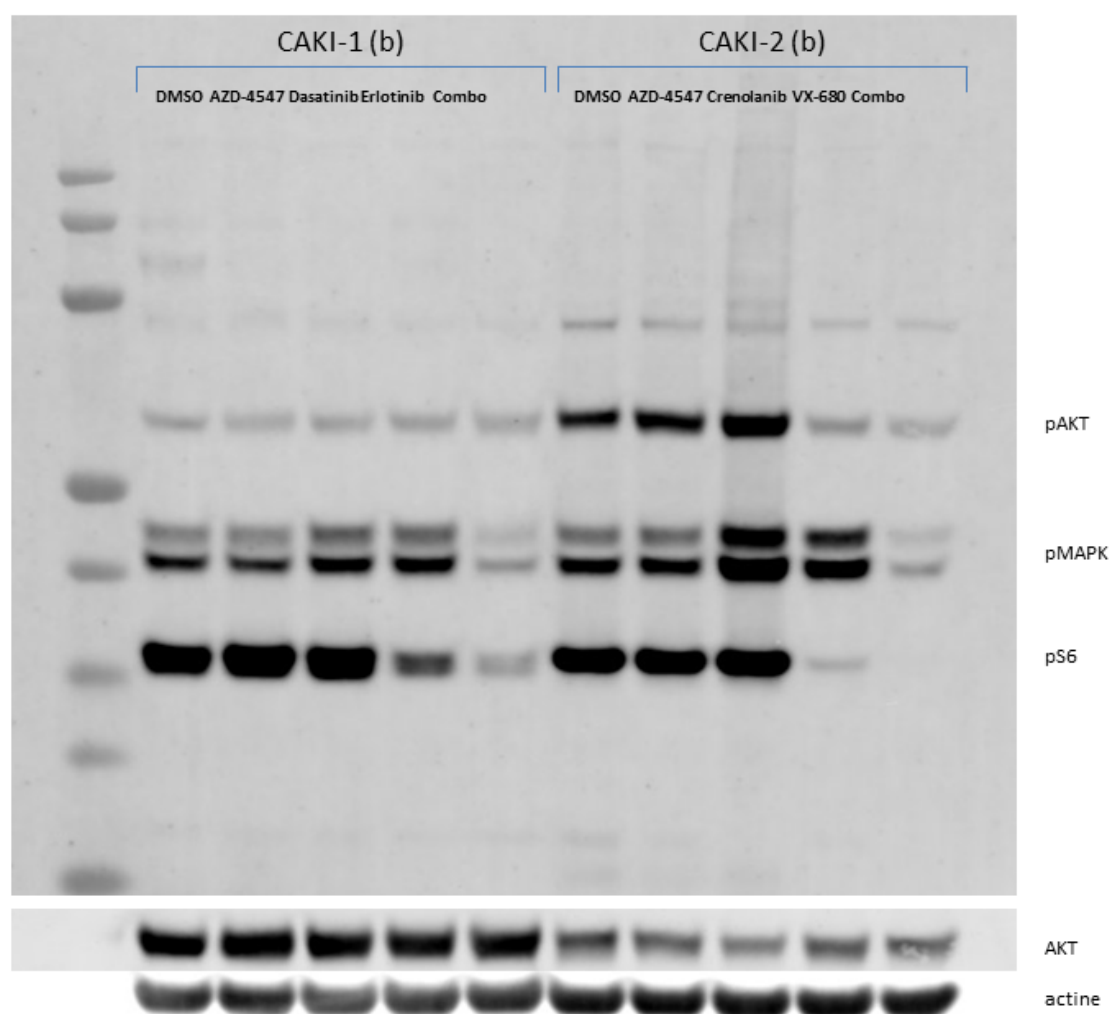
**Figure S8.** Heatmap of  $\text{EC}_{50}$  of drugs inhibiting most active 786-O kinases. Drugs with reported  $\text{EC}_{50} < 2\mu\text{M}$  against the top 20 INKA kinases in untreated 786-O were retrieved from proteomicsdb.org, and used for clustering and heatmap generation. Lighter colors indicate higher activity (higher  $-\text{Log}_{10}(\text{EC}_{50})$  values) against a given kinase. It shows that many drugs are effective against multiple kinases while others are relatively specific for a single kinase.

**Supplements 9–10: Western blot**

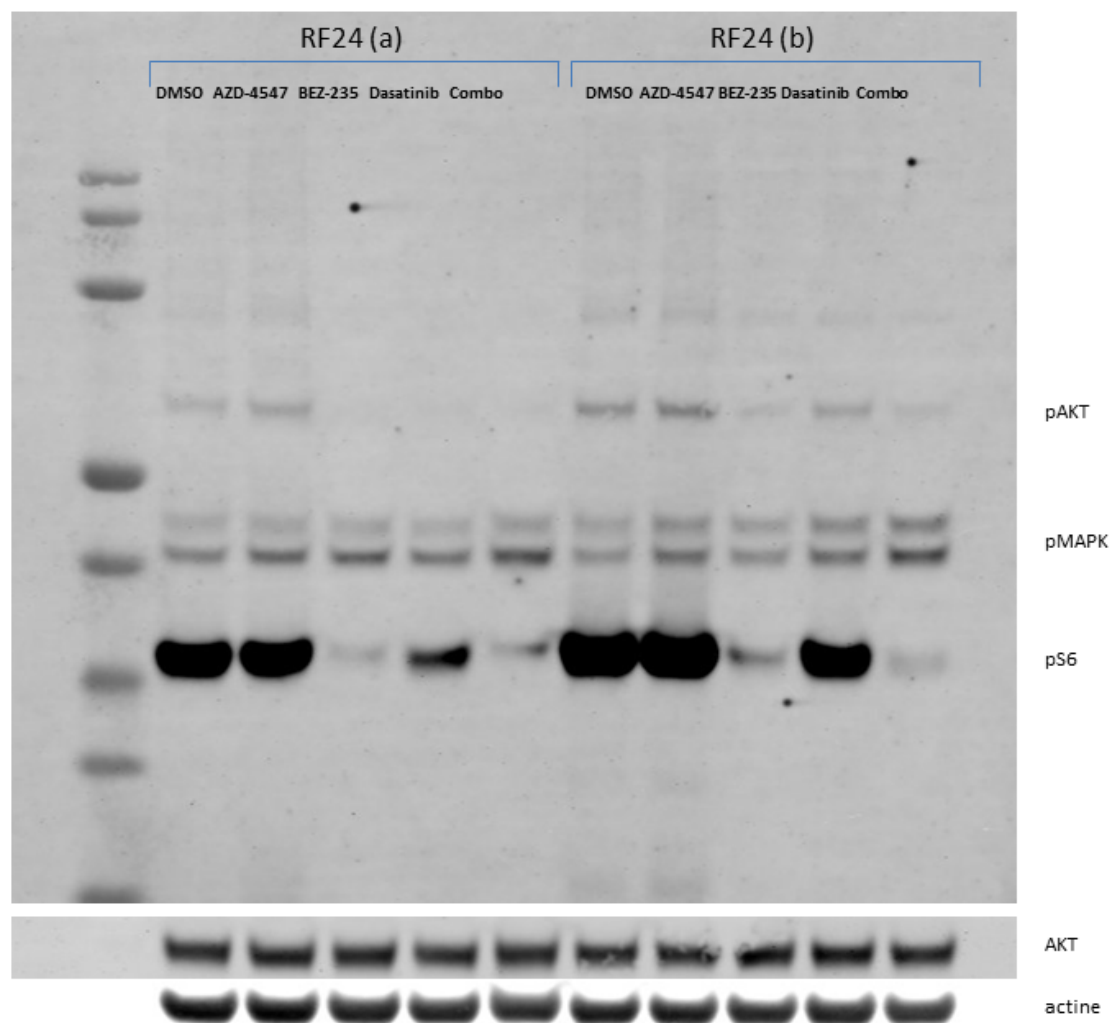
Figure S9.1–3: Original Western blot images and reference to Figure 2 and Figure S7.1



**Figure S9.1.** Detection of phosphor-AKT, phosphor-MAPK and phosphor-RPS6 in 786-O and A498 as presented in Figure 2.



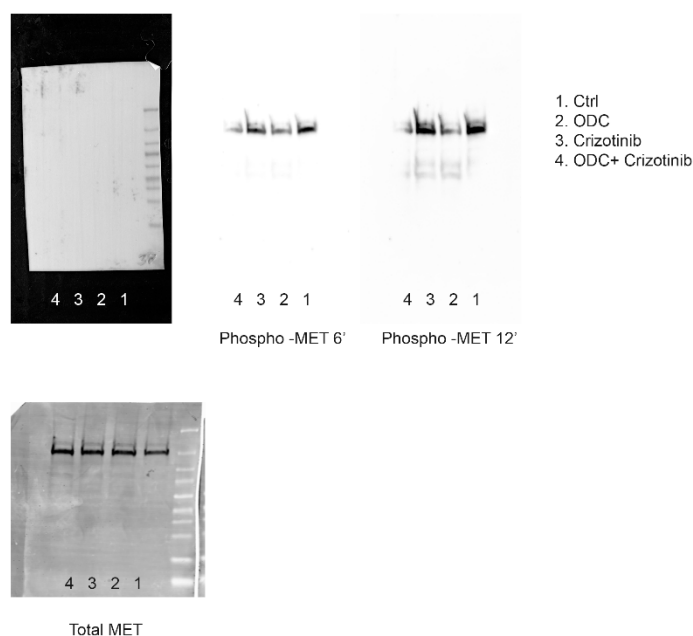
**Figure S9.2.** Detection of phosphor-AKT, phosphor-MAPK and phosphor-RPS6 in Caki-1 and Caki-2 as presented in Figure 2.



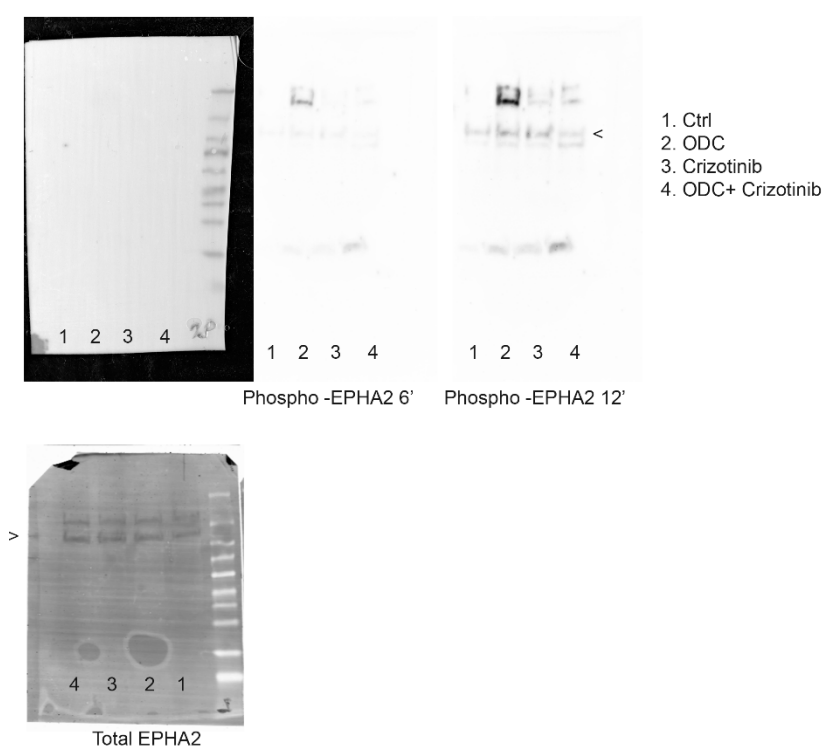
**Figure S9.3.** Detection of phosphor-AKT, phosphor-MAPK and phosphor-RPS6 in duplicate samples RF24 of which the left is presented in Figure S7.1

Figure S10.1–4. Original Western blot images and reference to main figure 6.

Original blots. Lane numbers are indicated and may be mirrored in the presentation of figure 6. Furthermore, for adequate presentation in main figure 6, contrast was globally adjusted.



**Figure S10.1.** MET: For phosphoMET, exposure of 6' is presented in Fig 6. It must be noted that due to the low expression of phosphoMET, blots were developed using a Uvitec Alliance chemiluminescence imager whereas the remainder of the blots were imaged using Licor Odyssey CLx scanner. Therefore, a separate (light) image is shown of the blot to show the molecular weight marker.



**Figure S10.2.** EPHA2: For phosphoEPHA2, exposure of 12' is presented in Fig 6. It must be noted that due to the low expression of phosphoEPHA2, blots were developed using a Uvitec Alliance chemiluminescence imager whereas the remainder of the blots were imaged using Licor Odyssey CLx scanner. Therefore, a separate (light) image is shown of the blot to show the molecular weight marker. The correct MW band of EPHA2 is indicated with ">".

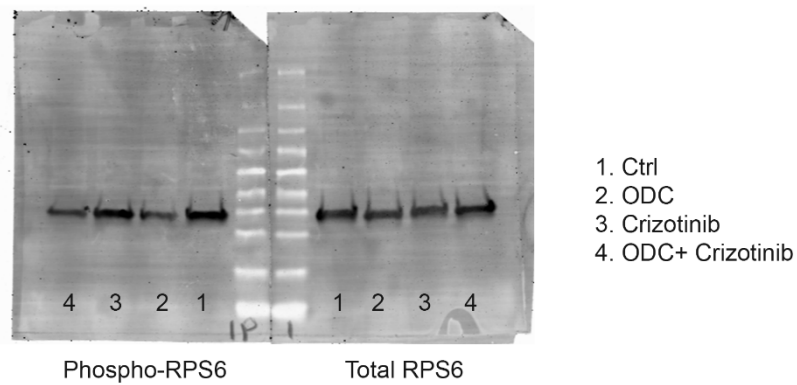


**Figure S10.3.** RPS6

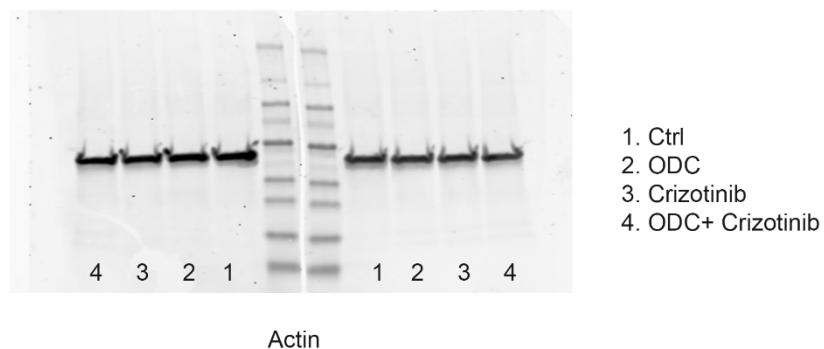


**Figure S10.4.** Actin: Two blots are shown as separate blots were probed for total and phosphoprotein in the experiments.